Frontiers in Heat and Mass Transfer

Available at www.ThermalFluidsCentral.org

ENTROPY GENERATION OF THREE DIMENSIONAL BINGHAM NANOFLUID FLOW WITH CARBON NANOTUBES PASSING THROUGH PARALLEL PLATES

P.S.S. Nagalakshmi and N. Vijaya[*]

Department of Engineering Mathematics, College of Engineering, Koneru Lakshmaiah Education Foundation, Vaddeswaram, A.P, India -522502.

ABSTRACT

The main emphasis of this study is to examine the entropy generation of the spatial-temporal state of Bingham visco-plastic nanofluid flow between parallel plates are solved numerically using adequate similarity solutions. Python with BVP solver is used to interpret the results of the adopted model. Heat and mass transfer rate with respect to yield stress was investigated. The results report that the entopy generation of nanofluids exploring single and multiwalled carbon nanotubes dims with the increasing local thermal Peclet number nearer the lower and upper plates. Researchers have established that entropy generation can be reduced by increasing Fourier's number (Fe) in nanofluids containing single- and multi-walled carbon nanotubes. Additionally, these results show that the heat transfer rate from water base CNTs to upper plate increases with raising local thermal transfer Peclet number and Fourier number.

Keywords: *SWCNT, MWCNT, Yield stress, Activation energy, Thermal radiation.*

1. INTRODUCTION

In materials science and engineering, the limit of stretchability behavior and the beginning of plastic behavior were decided by the yield point on a stress-strain curve. Bingham fluids exhibit the behavior of visco-plastic nature. If the shear stress exceeds a yield value, and like a stubborn otherwise. By adopting the fixed point method and saddle point method, Sanchez (1998) simulates the flow of a Bingham visco-plastic flow problem. Comparini and Mannucci (1998) analyzes the boundary value problem of Binham fluid flow in terms of lubrication. Huilgol and Mena (2000) describes how the Laplacian method was used to solve the problem of unsteady pipe flow in Bingham fluid. In Alexandrou *et al.* (2001), Reynolds and Bingham's numbers were investigated in the context of turbulent flow through a two-dimensional cavity under inertial, viscous, and yield stresses. The second-order linear differential operator was used to calculate the Couette flow of a Bingham fluid when density, viscosity, and yield stress are considered in Huilgol *et al.* (2002). In Zhang *et al.* (2002), Bingham plastic fluid under yield stress was studied in a parallel channel. It has been shown in Busuioc and Cioranescu (2003) that the upper bound for stopping time for a Bingham fluid is exhibited by an electric field. The hydrodynamic benchmark of the lid-driven cavity and the natural convection benchmark of the differentially heated cavity model of unsteady flows of Bingham fluids was computed in Vola *et al.* (2003). Bingham fluid behaves like a Newtonian fluid throughout the flow region due to yield stress was concluded in Huilgol (2004).

Bingham fluid between parallel plates model problem reduces to that of a Newtonian fluid when the yield stress is equal to zero was observed in Chen *et al.* (2004). Bingham fluid through arrays of aligned cylinders is identically equal to the sum of the drag forces of Newtonian and perfectly plastic fluids were obtained in Spelt *et al.* (2005). Axial and radial flow impellers in a tank of Heinz ketchup of Bingham plastic fluids to predict the cavern diameter and cavern height within the experimental uncertainty were interpreted by Wilkens *et al.* (2005). The distance between the parallel plates is small compared to the plate radius to minimize an energy dissipation functional of extensional Bingham fluid flow model was analyzed by Roussel *et al.* (2006). The radial velocities and pressure gradients in the Newtonian part with high viscous Newtonian fluid and a bi-viscosity part with yielded/unyielded Bingham fluid Navier slip condition were discussed in Yang and Zhu (2006). The heat transfer performance of the gel is modeled as a Bingham material between two parallel plates as described in Bayazitoglu *et al.* (2007). Effect of uniform magnetic field on velocity, temperature, and heat transfer rate of Bingham fluid over a porous rotating disk in the presence of Hall and ion-slip currents was computed in Osalusi *et al.* (2007). Bingham fluid flow between two porous parallel plates strongly depends on slip parameter as compared to Bingham number, Couette number, and transverse Reynolds number was observed in Chen and Zhu (2008). Interpretations can be done through log-log plotsOwayed and Tiab (2008) to analyze the pressure and pressure derivative behavior of Bingham fluid for horizontal

---

[†]*Corresponding author. Email: vijayanalleboyina@kluniversity.in*

wells. Correlations between the drag coefficient and the stability crite- rion with a high yield stress of Bingham viscoplastic fluid flow between two circular cylinders were solved numerically using the finite element method in Tokpavi et al. (2009). The load-bearing capacity of bubble min WANG et al. (2009) is enhanced with an increase in the magni- tude of viscosity of the Bingham fluid. General Herschel–Bulkley model of Lagrangian approach to Bingham fluid flow was numerically solved in Zhang (2010). Smoothed particle hydrodynamics (SPH) method was adopted to compute stress, strain rate and velocity profiles of Bingham- like fluids in two-dimensional vane and cylinder rheometers Zhu et al. (2010). The effect of Bingham number and also the gap size of two concentric cylinders on Taylor–Dean flow and Dean flow Soleimani and Sadeghy (2011) of Bingham fluid was solved by the pseudo-spectral col- location method. Streamlines and yielded/unyielded regions of Bingham flow over a cavity using the lattice Boltzmann method were investigated in Tang et al. (2011). Pressure gradient along the closed pipe Oliveira et al. (2012) of Bingham fluid correlate with yield stress, pipe aspect ratio, the Reynolds and Mach numbers. Bingham fluid allows for a two-scale approach (Ratio of width and length of channel) by a pressure gradient was studied in Fusi et al. (2012).

In this modern world of industrialization, vast empirical and theo- retical explorations are dealt on nanofluids especially in the heat transfer field. The term "nanofluid" was first identified by Choi and Eastman. Nanofluids are prepared as engineered colloidal suspension of nanome- ter sized tiny particles into a solvents. According to basic wave theory nano particles is typically observed between near infrared to thermal in- frared band under electromagnetic spectrum. The particle size is gen- erally in the range of 10-100nm. In recent years, few experiments and numerical simulations have been carried out to study nanofluid flow de- formation. Hydro magnetic unsteady channel flow of nanofluid was nu- merically analysed by Awan et al. (2018) . Nanofluid with mixed bio- convection was carried out by Kumar et al. (2019). Few applications of nanofluids in cooling eclecronic components, refrigeration refrigera- tion systems Jiang et al. (2022), car radiator coolants, engine coolants, cooling and drying of paper and textiles, energy harvesting approaches such as alternative energy, nuclear energy, geothermal energy, solar en- ergyChavez Panduro et al. (2022), batteries, and fuel cells as well as oil Hussain et al. (2022)and gas. The boundary layer flow has been a keen interest of study in view of its nanofluid applications. Nanofluid bound- ary value problem with the effect of biot-number and slip paramter was explained by Ali et al. (2022). Heat and mass transfer rate of Maxwell nanofluid was computed in Ahmad et al. (2021). Casson nanofluid with radiative slip was analysed by Liu et al. (2021). William sons flow with mixed convection was solved bySong et al. (2022). Nanofluid flow with differnt shapes of concrete cylinder was studied by Aboud et al. (2021) . Heat and mass transfer effect of nanofluid flow through multi junction solar cell was investigated in Hasan et al. (2022). Experimental study on nanofluid in crude oil heating furnance was oberved by Yun et al. (2022).

It has been shown that Bingham's nanofluids can be investigated in a number of different rheological states using numerical and practi- cal methods, but this paper reveals an innovative structure of governing equations with adequate similarity variables. As of yet, however, there is scant information regarding the heat and mass transfer rates and the entropy generation of Bingham's nanofluids using carbon nanotubes be- tween parallel plates under the influence of local Peclet numbers, local concentration Peclet numbers, thermal Fourier numbers, and concentra- tion Fourier numbers. Moreover, this exploration becomes unique when the above features are paired with the nanothermophysical properties of base fluids explored with SWCNT and MWCNT. The erected model is then numerically solved using a built-in Python function with BVP solver.

2. MATHEMATICAL FORMULATION

The researchers are exploring a three-dimensional flow of Bingham nanofluid using CNTs between two parallel plates with pressure gradients. Visco-
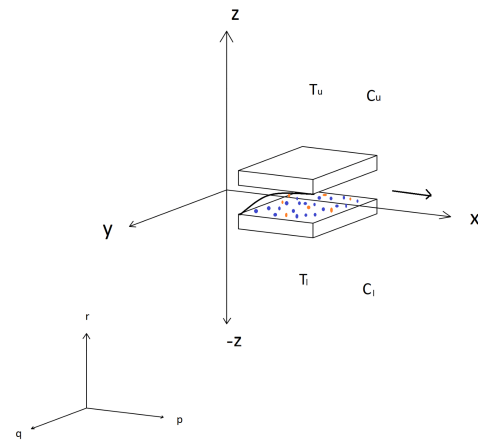

Fig. 1 Flow diagram.

plastic nature of three-dimensional unsteady flow of nanofluid will occur when the parallel plates are kept at the XY plane with z=-h1 and z=h1. Let p=P=p_w, q=Q=q_w, T=T_u, and C=C_u be the velocities, temperature, and concentration of the nanofluid near the upper plate having z=h1, and T=T_l, and C=C_l be the temperature, and concentration of the nanofluid near the lower plate having z=-h1.Where h1 is the height of the plates from origin. Magnetic field and electric field parameters are the func- tions of the temporal state. Moreover, investigators assume that the spa- tiotemporal state of Bingham's nanofluid with activation energy and joule heating can be written as Islam et al. (2019):

$$\frac{\partial p}{\partial x} + \frac{\partial q}{\partial y} + \frac{\partial r}{\partial z} = 0 \qquad (1)$$

$$
\begin{aligned}
\frac{\partial p}{\partial t} &+ p\frac{\partial p}{\partial x} + q\frac{\partial p}{\partial y} + r\frac{\partial p}{\partial z} = \\
\frac{\partial p}{\partial t} &+ p\frac{\partial p}{\partial x} \\
&- \frac{p\sigma_{nf}}{\rho_{nf}}B^2(t) + \frac{\sigma_{nf}}{\rho_{nf}}E(t)B(t) \\
&- \left[\frac{c_b}{(k^*)^{1/2}}p - \frac{\nu_{nf}}{k^*}\right]p \\
&+ g\frac{(\rho\beta_T)_{nf}}{\rho_{nf}}(T - T_u) + g\frac{(\rho\beta_c)_{nf}}{\rho_{nf}}(C - C_u) \\
&+ \frac{\mu_{nf}}{\rho_{nf}}\left[\frac{\partial}{\partial x}\left(2\frac{\partial p}{\partial x} - \frac{2}{3}\left(\frac{\partial p}{\partial x} + \frac{\partial q}{\partial y} + \frac{\partial r}{\partial z}\right)\right)\right] \\
&+ \frac{\mu_{nf}}{\rho_{nf}}\left[\frac{\partial}{\partial y}\left(\frac{\partial p}{\partial y} + \frac{\partial q}{\partial x}\right)\right] \\
&+ \frac{\mu_{nf}}{\rho_{nf}}\left[\frac{\partial}{\partial z}\left(\frac{\partial r}{\partial x} + \frac{\partial p}{\partial z}\right)\right]
\end{aligned}
\qquad (2)
$$

$$
\begin{aligned}
\frac{\partial q}{\partial t} &+ p\frac{\partial q}{\partial x} + q\frac{\partial q}{\partial y} + r\frac{\partial q}{\partial z} = \\
\frac{\partial Q}{\partial t} &+ Q\frac{\partial Q}{\partial y} \\
&+ \frac{\mu_{nf}}{\rho_{nf}}\left[\frac{\partial}{\partial y}\left(2\frac{\partial q}{\partial y} - \frac{2}{3}\left(\frac{\partial p}{\partial x} + \frac{\partial q}{\partial y} + \frac{\partial r}{\partial z}\right)\right)\right] \\
&+ \frac{\mu_{nf}}{\rho_{nf}}\left[\frac{\partial}{\partial z}\left(\frac{\partial q}{\partial z} + \frac{\partial r}{\partial y}\right) + \frac{\partial}{\partial x}\left(\frac{\partial p}{\partial y} + \frac{\partial q}{\partial x}\right)\right]
\end{aligned}
\qquad (3)
$$

$$\frac{\partial T}{\partial t} + p\frac{\partial T}{\partial x} + q\frac{\partial T}{\partial y} + r\frac{\partial T}{\partial z} =$$

$$\alpha_{nf}\left[\frac{\partial^2 T}{\partial x^2} + \frac{\partial^2 T}{\partial y^2} + \frac{\partial^2 T}{\partial z^2}\right] - \frac{\partial q_r}{\partial z}$$

$$-\frac{\mu_{nf}}{(\rho c p)_{nf}}\left[\frac{2}{3}\left[\left(\frac{\partial p}{\partial x} + \frac{\partial q}{\partial y} + \frac{\partial r}{\partial z}\right)^2\right]\right]$$

$$-\frac{\mu_{nf}}{(\rho c p)_{nf}}\left[\frac{2}{3}\left[\left[\frac{\partial p}{\partial y} + \frac{\partial q}{\partial x}\right]^2\right]\right] \tag{4}$$

$$+\frac{\mu_{nf}}{(\rho c p)_{nf}}\left[2\left(\left(\frac{\partial p}{\partial x}\right)^2 + \left(\frac{\partial q}{\partial y}\right)^2 + \left(\frac{\partial r}{\partial z}\right)^2\right)\right]$$

$$+\frac{\mu_{nf}}{(\rho c p)_{nf}}\left[\frac{2}{3}\left[\frac{\partial q}{\partial z} + \frac{\partial r}{\partial y}\right]^2 + \left[\frac{\partial r}{\partial y} + \frac{\partial p}{\partial z}\right]^2\right]$$

$$+\frac{\sigma_{nf}}{(\rho c p)_{nf}}(pB(t) - E(t))^2 + \frac{Q_0(T - Tu)}{(\rho c p_{nf})}$$

$$\frac{\partial C}{\partial t} + p\frac{\partial C}{\partial x} + q\frac{\partial C}{\partial y} + r\frac{\partial C}{\partial z} =$$

$$\frac{(D_T)_{nf}}{T_u}\frac{\partial^2 T}{\partial z^2}$$

$$+ (D_B)_{nf}\frac{\partial^2 C}{\partial z^2} \tag{5}$$

$$- K_r^2\left(\frac{T}{T_u}\right)^{n1} exp\left(\frac{-E}{KT}\right)(C - C_u)$$

$$where \quad B(t) = \frac{B_0}{\sqrt{1-\beta t}}, E(t) = \frac{E_0}{\sqrt{1-\beta t}}$$

Subject to

$$p = 0 = q = r, \quad T = T_l, \quad C = C_l \quad at \quad z = -h1,$$

$$p = P = \frac{ax}{1-\beta t}, \quad q = Q = \frac{by}{1-\beta t}, \quad r = 0, \quad at \quad z = h1 \tag{6}$$

$$T = T_u, \quad C = C_u \quad at \quad z = h1$$

Similarity Variables

$$p = \frac{ax}{1-\beta t}f^1(\mu), \quad q = \frac{ay}{1-\beta t}g^1(\mu), \quad r = \frac{-ah1}{1-\beta t}(f+g)$$

$$\eta = \frac{z}{h_1}, \quad \theta = \frac{T-T_l}{T_u-T_l}, \quad h = \frac{C-C_l}{C_u-C_l} \tag{7}$$

Nanofluid Parameters

$$\mu_{nf} = \frac{\mu_f}{(1-\phi)^{2.5}} \quad ; where \quad \mu_f = \mu_p + \frac{\tau_b}{\frac{\partial p}{\partial z}}; \quad \nu_{nf} = \frac{\mu_{nf}}{\rho_{nf}} \quad ;$$

$$\rho_{nf} = (1-\phi)\rho_f + \phi\rho_{CNT};$$

$$(\rho c_p)_{nf} = (1-\phi)(\rho c_p)_f + \phi(\rho c_p)_{CNT};$$

$$\frac{K_{nf}}{K_f} = \frac{(1-\phi)(K_{CNT}-K_f) + 2\phi K_{CNT}\ln(\frac{K_{CNT}+K_f}{2K_f})}{(1-\phi)(K_{CNT}-K_f) + 2\phi K_f\ln(\frac{K_{CNT}+K_f}{2K_f})};$$

$$\frac{\sigma_{nf}}{\sigma_f} = 1 + \frac{3(\sigma_{CNT}-\sigma_f)\phi}{(\sigma_{CNT}+2\sigma_f) - (\sigma_{CNT}-\sigma_f)\phi};$$

$$(\rho\beta_T)_{nf} = (\rho\beta_T)_f(1-\phi) + (\rho\beta_T)_{CNT}\phi;$$

$$D_{nf} = (1-\phi)D_f \quad ; \quad (\rho\beta_c)_{nf} = (\rho\beta_c)_f(1-\phi) + (\rho\beta_c)_{CNT}\phi \tag{8}$$

ODE

$$(f^1)^2 - (ff^{11} + gf^{11}) + unf^1 - un - 1 - \frac{A_3}{A_2}M_1E_1 + \frac{A_3}{A_2}M_1f^1$$

$$- F_n(f^1)^2 + \frac{A_1}{A_2}\lambda\left[1 + \frac{\tau_B}{f^{11}}\right]f^1 - \frac{A_4}{A_2}Gr_x(\theta - 1)$$

$$- \frac{A_5}{A_2}Gc_x(h - 1) - \left[1 + \frac{\tau_B}{f^{11}}\right]\left[\frac{A_1}{A_2}\right]\frac{1}{Re}f^{111}(\eta) = 0 \tag{9}$$

$$\frac{A_1}{A_2}\left[1 + \frac{\tau_B}{f^{11}}\right]\frac{1}{Re}g^{111} + (1+un)\alpha - (g^1)^2 + fg^{11} + gg^{11} - (un)g^1 = 0 \tag{10}$$

$$\frac{A_6}{A_7}\left(1 + \frac{R}{A_6}\right)\frac{1}{(Pr)(Re)}\theta^{11} + \frac{2A_1}{A_7}\frac{1}{Re_x}Ec_x\left[1 + \frac{\tau_B}{f^{11}}\right]((f^1)^2 + (g^1)^2$$

$$+ (f^1 + g^1)^2) - \frac{2A_1}{A_7}\frac{1}{Re}\left[1 + \frac{\tau_B}{f^{11}}\right](Ec_x(f^{11})^2 + Ec_y(f^{11})^2)$$

$$+ (M_1)(Ec_x)/(f^1 - E_1)^2\frac{A_3}{A_4} + \frac{\lambda_1}{A_4}(\theta - 1) + \theta^1(f + g) = 0 \tag{11}$$

$$(1-\phi)\left[\left(\frac{Nt}{Nb}\right)\left(\frac{1}{Re}\right)\theta^{11} + \frac{1}{Re}h^{11}\right]$$

$$- K_R(Le)(Pr)(h - 1)\left(\delta 1 + (1-\delta 1)\theta\right)^{n1}e^{\left(\frac{-En}{1+\left(\frac{1}{\delta 1}-1\right)\theta}\right)} \tag{12}$$

$$+ Sc(f + g)h_1 = 0$$

Subject to

$$f^1(\eta) = 0, \quad g^1(\eta) = 0, \quad \theta = 0,$$

$$h = 0 \quad at \quad \eta = -1 \quad ; \quad f^1(\eta) = 1, \tag{13}$$

$$g^1(\eta) = \alpha, \quad \theta = 1, \quad h = 1 \quad at \quad \eta = 1$$

Thermo physical parameters

$$A_1 = \frac{1}{(1-\phi)^{2.5}} \quad , A_2 = (1-\phi) + \frac{\rho_{CNT}}{\rho_f}\phi,$$

$$A_3 = 1 + \frac{3(\sigma_{CNT} - \sigma_f)\phi}{(\sigma_{CNT} + 2\sigma_f) - (\sigma_{CNT} - \sigma_f)\phi} \quad ,$$

$$A_4 = (1-\phi) + \frac{(\rho\beta_T)_{CNT}}{(\rho\beta_T)_f}\phi,$$

$$A_5 = (1-\phi) + \frac{(\rho\beta_c)_{CNT}}{(\rho\beta_c)_f}\phi,$$

$$A_6 = \frac{(1-\phi)(K_{CNT} - K_f) + 2\phi K_{CNT}\ln(\frac{K_{CNT}+K_f}{2K_f})}{(1-\phi)(K_{CNT} - K_f) + 2\phi K_f\ln(\frac{K_{CNT}+K_f}{2K_f})},$$

$$A_7 = (1-\phi) + \frac{(\rho c_p)_{CNT}}{(\rho c_p)_f}\phi,$$

$$un = \frac{\beta}{a}, \quad M1 = \frac{\sigma_f B_0^2}{\rho_f a}, \quad E1 = \frac{E_0}{B_0 P}, \quad Fn = \frac{C_b x}{(k^*)^{\frac{1}{2}}}, \quad \tau_B = \frac{\tau_b h_1}{\mu_p P},$$

$$\lambda = \frac{\mu_p x}{\rho_f k^* P}, Gr_x = \frac{g(B_T)_f\Delta T}{p^2}x, \quad Gc_x = \frac{g(B_c)_f\Delta c}{\rho_f p^2}x, \quad R = \frac{16\sigma^* T\infty^3}{3K^s K_f}$$

$$Re = \frac{\rho_f ah1^2}{\mu(1-\beta t)}, \quad \alpha = \frac{b}{a}, \quad \lambda_1 = \frac{Q_0(1-\beta t)}{a(\rho C_p)f}, \quad Pr = \frac{\nu f}{\alpha_f};$$

$$Ec_x = \frac{P^2}{(C_P)_f\Delta T}, Ec_y = \frac{Q}{(C_P)_f\Delta T}, \quad Re_x = \frac{Px}{\nu_f}, \quad Re_y = \frac{Qy}{\nu_f}$$

$$Nt = \frac{(D_T)_f\Delta T}{T_u\nu_f}, \quad Nb = \frac{(D_B)_f\Delta C}{\nu_f}, \quad Sc = \frac{\nu}{(D_B)_f}, \quad Le = \frac{\alpha_f}{(D_B)_f},$$

$$KR = \frac{(1-\beta t)(k_r)^2}{a}, \quad En = \frac{E}{KT_l}, \quad \delta 1 = \frac{T_l}{T_u} \tag{14}$$

Engineering Parameters

$$C_{fx} = \frac{\tau_{wx}}{\frac{1}{2}\rho_{nf}p_w^2}, \quad C_{fy} = \frac{\tau_{wy}}{\frac{1}{2}\rho_{nf}p_w^2}$$

$$\tau_{wx} = \mu_{nf}\left[\frac{\partial p}{\partial z} + \frac{\tau}{\sqrt{2}}(\frac{\partial p}{\partial z})^2\right]_{z=h1}, \quad \tau_{wy} = \mu_{nf}\left[\frac{\partial q}{\partial z} + \frac{\tau}{\sqrt{2}}(\frac{\partial q}{\partial z})^2\right]_{z=h1}$$

$$Nu_x = \left[-\frac{x}{(T_l - T_w)}\frac{\partial T}{\partial z} + \frac{xq_r}{k_{nf}(T_l - T_w)}\right]_{z=h1}$$

$$q_r = -\frac{16\sigma^*T_\infty^3}{3k^*}\frac{\partial T}{\partial z}, Sh_x = -\left[\frac{x}{(C_w - C_\infty)}\frac{\partial C}{\partial z}\right]_{z=h1}$$

$$C_{fx} = 2\frac{A_1}{A_2}\frac{1}{Re_x}\left(1 + \frac{\tau_B}{f^{11}(1)}\right)\left[f^{11}(1)\right]$$

$$C_{fy} = 2\frac{A_1}{A_2}\frac{1}{Re_y}\left(1 + \frac{\tau_B}{f^{11}(1)}\right)\left[g^{11}(1)\right]$$

$$Nu_x = Pe_xFe \quad (1 - \frac{Ra}{A_6})\theta^1(1)$$

$$Sh_x = Pe_{xm}(Fe_m) \quad h^1(1)$$

$$Pe_x = \frac{Px}{\alpha_f}, \quad Fe = \frac{\alpha_f}{(P)(h1)}, \quad Pe_{xm} = \frac{Px}{D_f}, \quad Fe_m = \frac{D_f}{(P)(h1)}$$

(15)

Spatial simulation for Entropy Generation

$$en_{gen} = \frac{K_{nf}}{T_\infty^2}\left(\frac{\partial T}{\partial z}\right)^2 - \frac{1}{T_u}\frac{\partial q_r}{\partial z}$$

$$+ \frac{\mu_{nf}}{T_u}\left(2\left(\frac{\partial p}{\partial x}\right)^2 + 2\left(\frac{\partial q}{\partial y}+\right)^2 + 2\left(\frac{\partial r}{\partial z}+\right)^2\right) \quad (16)$$

$$+ \frac{\sigma_{nf}}{T_u}(pB_0 - E_0)^2 + \frac{D_B}{T_\infty}\frac{\partial T}{\partial y}\frac{\partial C}{\partial y} + \frac{D_B}{C_\infty}\left(\frac{\partial C}{\partial y}\right)^2$$

The dimesionless entropy generation of the spatial mathematical model has been deduced from the similarity variales can be written as

$$En_{gen} = A6\left(\theta^1\right)^2 + \frac{R}{1-\delta1}\theta^1$$

$$+ \frac{4A1}{1-\delta1}\frac{Bk_1}{(Pe_xFe)^2}\left(1 + \frac{\tau_B}{f^{11}}\right)\left[\left(f^1\right)^2 + \left(g^1\right)^2 + f^1g^1\right]$$

$$+ \frac{Bk_1}{1-\delta1}(Ha)(A3)\left(f^1 - E1\right)^2$$

$$+ (1-\phi)\frac{d_p}{1-\delta1}\theta^1h^1 + (1-\phi)\frac{d_p}{(1-\delta1)^2}\delta2(h^1)^2$$

(17)

where

$$En_{gen} = \frac{en_{gen}T_u^2h1^2}{(\Delta T)^2 K_f}, \quad Ha = \frac{\sigma_f B_0^2h^2}{\mu_p}, \quad Bk_1 = \frac{\mu_pP^2}{K_f(\Delta T)},$$

$$Pe_x = \frac{xP}{\alpha_f}, \quad Fe = \frac{\alpha_f}{Ph1}, \quad d_p = \frac{D_B\Delta C}{K_f}, \quad \delta2 = \frac{\Delta C}{C_u}$$

(18)

Here E_{gen} is the entropy generation rate, Ha is the Hartman number ,Bk_1 is the Brihkman number which represents the ratio of the viscous entropy generation to thermal entropy generation, Pe_x is the local heat transfer Peclet number, Fe is the Fourier number ,d_p is the diffusion parameter, $\delta2$ is the concentration difference parameter respectively.

Threshold values of thermo-physical parameters

$$M1 = 2; E1 = 0.5; Fn = 0.2; \tau_B = 0.5; Gr_x = 0.2; Gc_x = 0.1;$$

$$\lambda = 0.1; un = 0.1; \alpha = 1; \lambda1 = 0.1; R = 0.4; Pr = 6.9;$$

$$Sc = 2; Nt = 0.01; Nb = 0.6; \delta1 = 1; En = 1; n1 = 0.5;$$

$$Le = 0.01; KR = 0.3; Re_x = 3; Re_y = 2; Re = 2;$$

$$Ec_x = 1e - 3; Ec_y = 0.1; \phi = 0.1; Pe_x = 2; Pe_{xm} = 4;$$

$$Fe = 2; Fe_m = 3; Ha = 3; Bk1 = 0.05; d_p = 0.5; \delta2 = 0.5;$$

(19)

3. RESULTS AND DISCUSSION

Influence of SWCNT, MWCNT with different base fluids of a two-parallel plate system is used in this study to investigate the properties of carbon nanotubes on Bingham nanofluid. Modern ODEs can now be solved with Python and BVP schemes. We examine momentum, thermal, and concentration boundary layers from the viewpoint of the thermophysical properties of SWCNT and MWCNT. Causs and effect relation between magnetic parameter(M1), electric parameter(E1), thermal radiation(R), local thermal Grashof Number(Gr_x), local concentration Grashof Number (Gc_x), heat source parameter ($\lambda1$), buoyancy(λ), Inertia-coefficient(Fn), volume fraction of nanoparticle(ϕ), Smidth number(Sc) , temperature difference parameter($\delta1$), activation energy number(En) on momentum, thermal, and concentration profiles are depicted through graphs using python with boundary value problem solver. Estimated heat and mass transfer rates of the adopted mathematical model about local thermal Peclet number (Pe_x), local mass transfer Peclet number (Pe_{xm}), and heat transfer Fourier number (Fe), and mass transfer Fourier number(Fe_m) are observed in tables. For determining the convergence of boundary layers, thermophysical parameters (from equation 19) are used as threshold values.

Fig. 2 shows that retardation occurs when increasing the magnetic parameter(M1), but the reverse tendency happens with the rising of the electric parameter(E1),λ, and Fn.

Fig. 3 demonstrate deceleration happened with increasing Gr_x and Gc_x near the lower plate. Fig. 4 depicts vertical velocity decrease with increasing E1, λ, and Fn but the opposite tendency occurs due to M1 at the upper plate. Nearer lower plate the vertical velocity increases with increasing Gr_x and Gc_x are shown in Fig. 5.

Fig. 6 demonstrates the temperature increases with increasing E1, λ, Fn but the opposite tendency occurs with the rise of M1 nearer to the lower plate. Temperature decreases with increasing Gr_x and Gc_x at the lower plate as observed in Fig. 7. Temperature decreases with increasing $\lambda1$ but increases with increasing R at the lower plate, in addition to this temperature increases with increasing R but decreases with increasing $\lambda1$ nearer to the upper plate as shown in Fig. 8.

The concentration of nanoparticles decreases with increasing M1 and increases with increasing E1 as shown in Fig. 9 nearer to the lower plate. The concentration of the nanoparticles nearer to the lower plate decrease with increasing Gr_x, Gc_x, and λ but the opposite tendency occurs with increasing Fn as shown in Fig. 10.

The concentration of nanoparticles nearer to the lower plate decreases with increasing Le,Nt, KR, and n1 but the opposite tendency occurs with increasing Sc, Nb, and $\delta1$ as shown in Fig. 11.

Investigators concluded that the cause and effect relationship between noticed thermo physical parametes with the behaviour of nanofluid were good agrement with previously published papers.

Fig. 12 illustrates how the Bingham number influences the velocity profile. Bingham number is inversely proportional to fluid velocity near the lower plate. The explanation lies in the force of shear. As shown in Fig. 13, the vertical velocity profile exhibits the same impact. A lowered temperature profile is depicted in Fig. 14 with an increase in Bingham number. Thermal conduction of fluid from the upper plate causes the temperature near the lower plate to suddenly increase. Fig. 15 illustrates the increase in nanoparticle concentration on the lower plate associated with the rise in Bingham number. Shear stress plays a major role in reducing velocity, temperature, and concentration profiles.

Fig. 16, Fig. 17, Fig. 18, and Fig. 19 illustrate how the unsteady parameter(un) increases the momentum, temperature, and concentration of nanofluid. Increasing the coefficient of time enhances the momentum, thermal, and concentration of nanofluid on the bottom plate.

A decrease in velocity and temperature of nanofluid is observed when the volume fraction of nanofluid (ϕ) is raised, as shown in Fig. 20, Fig. 21, and Fig. 22. On the other hand, nanoparticle concentration rises near the bottom of the plate, as shown in Fig. 23.

A correlation between the activation energy parameters and nanofluid velocity, vertical velocity, temperature, and concentration is illustrated in Fig. 24, Fig. 25, Fig. 26, Fig. 27. The temperature and concentration of nanofluid increase with higher activation energy, however, the vertical velocity of nanofluid drops near the bottom plate. As a result, we can determine that the reaction rate parameter determines accelerated velocity, temperature, and concentration.

Fig. 28 illustrates that single-walled carbon nanotubes dominate engine oil velocity and the same trend can be seen in water under investigation with single-walled carbon nanotubes as opposed to multi-walled carbon nanotubes.

Fig. 29 also illustrates that single-walled carbon nanotubes are dominant when compared to multi-walled carbon nanotubes for nanofluids.

Nanofluids that use multiwalled carbon nanotubes to enhance the temperature of the fluid near the bottom of the plate are shown in Fig. 30

Comparing multi-walled nanotubes to single-walled nanotubes, Fig. 31 shows that nanofluids driven by single-walled nanotubes have higher concentrations near the bottom plate.

Fig. 32 illustrates nanofluids explored with single-walled carbon nanotubes that produce the most entropy near the bottom plate with the influence of Bingham number. Inadition to this entropy dicreses with increasing Bingham number at lower plate but contradictory results are obtained at upperplate. Thermal conduction of nanofluid at the upper plate is the main reason behind this effects.

Entopy generation of nanofluids explored with single and multi-walled carbon nanotubes dimnishes with the growth tendency of local thermal Peclet number nearer to the lower and upper plate are observed in Fig. 33. Thermal diffusivity of the base fluid is the cause of reduction of entropy generation.

Nanofluids with single-walled and multi-walled carbon nanotubes reduces entropy generation with increasing Fourier's number(Fe) as demonstrated in Fig. 34 at both lower and upper plates due to shear stress.

Based on Table 1 and 2, the coefficient of skin friction near the upper plate increases with increasing Bingham's number.

Table 3 illustrates that the rate of heat transfer from the fluid (water) to the upper plate is significantly affected by Bingham's number. Nonetheless, the rate of heat transfer decreases from engine oil to plate, enhancing Bingham's number.

According to Table 4, the rate of mass transfer increases near the upper plate by increasing Bingham's number with water and engine oil.

The rate of heat transfer from a fluid to a plate increases with an increasing local thermal Piclet number when the base fluid is water. If the base fluid is engine oil, the rate of heat transfer from the upper plate to the fluid decreases with increasing local Picklet number. A similar impact can be seen in Fourier's number.

As shown in Table 4, the rate of mass transfer increased near the upper plate with the enhancing mass transfer Piclet number and mass transfer Fourier's number based on water and engine oil were explored with carbon nanotubes.

Table 1 Influence of τ_B on cf$_x$

	τ_B=0.1	τ_B=0.2	τ_B=0.3	τ_B=0.4
Water	0.131039	0.19506	0.259582	0.324345
Water-SWCNT	0.150859	0.221662	0.293618	0.366015
Water-MWCNT	0.168108	0.244776	0.32321	0.402299
Engin oil	0.1301	0.196773	0.26309	0.329352
Engin oil-SWCNT	0.144269	0.21633	0.288434	0.360598
Engin oil-MWCNT	0.159935	0.239359	0.318925	0.398593

Table 2 Influence of τ_B on cf$_y$

	τ_B=0.1	τ_B=0.2	τ_B=0.3	τ_B=0.4
Water	-0.43186	-0.277928	-0.113273	0.060812
Water-SWCNT	-0.390633	-0.210779	-0.018082	0.185855
Water-MWCNT	-0.369001	-0.170423	0.043048	0.269295
Engin oil	-0.057171	-0.018979	0.022258	0.065231
Engin oil-SWCNT	-0.076822	-0.037279	0.004935	0.048075
Engin oil-MWCNT	-0.070192	-0.024409	0.02464	0.075088

Table 3 Influence of τ_B , Pe_x , and Fe on Nu$_x$

	τ_B=0.1	τ_B=0.2	τ_B=0.3	τ_B=0.4
Water	1.06012	1.06042	1.06073	1.06106
Water-SWCNT	1.0962	1.09642	1.09663	1.09685
Water-MWCNT	1.10152	1.10178	1.10202	1.10225
Engin oil	-3.01476	-3.04606	-3.05366	-3.0557
Engin oil-SWCNT	-0.754433	-0.760152	-0.753434	-0.743297
Engin oil-MWCNT	-1.33791	-1.33814	-1.32451	-1.30889
	Pe_x=1	Pe_x=2	Pe_x=3	Pe_x=4
Water	0.530697	1.06139	1.59209	2.12279
Water-SWCNT	0.548535	1.09707	1.64561	2.19414
Water-MWCNT	0.551246	1.10249	1.65374	2.20498
Engin oil	-1.52842	-3.05685	-4.58527	-6.11369
Engin oil-SWCNT	-0.365592	-0.731183	-1.09678	-1.46237
Engin oil-MWCNT	-0.646714	-1.29343	-1.94014	-2.58686
	Fe=1	Fe=2	Fe=3	Fe=4
Water	0.530697	1.06139	1.59209	2.12279
Water-SWCNT	0.548535	1.09707	1.64561	2.19414
Water-MWCNT	0.551246	1.10249	1.65374	2.20498
Engin oil	-1.52842	-3.05685	-4.58527	-6.11369
Engin oil-SWCNT	-0.365592	-0.731183	-1.09678	-1.46237
Engin oil-MWCNT	-0.646714	-1.29343	-1.94014	-2.58686

Table 4 Influence of τ_B , Pe_{xm} , and Fe$_m$ on Sh$_x$

	τ_B=0.1	τ_B=0.2	τ_B=0.3	τ_B=0.4
Water	2.96491	2.9689	2.97112	2.9726
Water-SWCNT	2.99133	2.99541	2.99769	2.99921
Water-MWCNT	2.99141	2.99525	2.99742	2.99887
Engin oil	1.51534	1.91757	2.06136	2.09617
Engin oil-SWCNT	1.30627	1.9574	2.30835	2.54113
Engin oil-MWCNT	1.45023	2.0213	2.30097	2.4567
	Pe_{xm}=1	Pe_{xm}=2	Pe_{xm}=3	Pe_{xm}=4
Water	0.743422	1.48684	2.23027	2.97369
Water-SWCT	0.750085	1.50017	2.25026	3.00034
Water-MWCNT	0.74999	1.49998	2.24997	2.99996
Engin oil	0.511554	1.02311	1.53466	2.04622
Engin oil-SWCNT	0.679047	1.35809	2.03714	2.71619
Engin oil-MWCNT	0.634273	1.26855	1.90282	2.53709
	Fe$_m$=1	Fe$_m$=2	Fe$_m$=3	Fe$_m$=4
Water	0.991229	1.98246	2.97369	3.96492
Water-SWCNT	1.00011	2.00023	3.00034	4.00045
Water-MWCNT	0.999987	1.99997	2.99996	3.99995
Engin oil	0.682072	1.36414	2.04622	2.72829
Engin oil-SWCNT	0.905396	1.81079	2.71619	3.62159
Engin oil-MWCNT	0.845698	1.69139	2.53709	3.38279
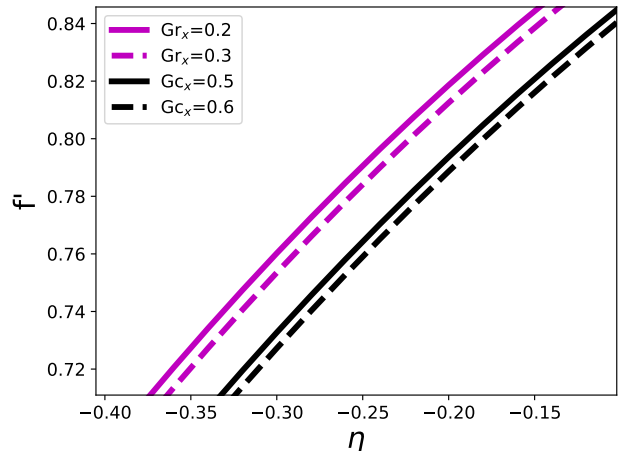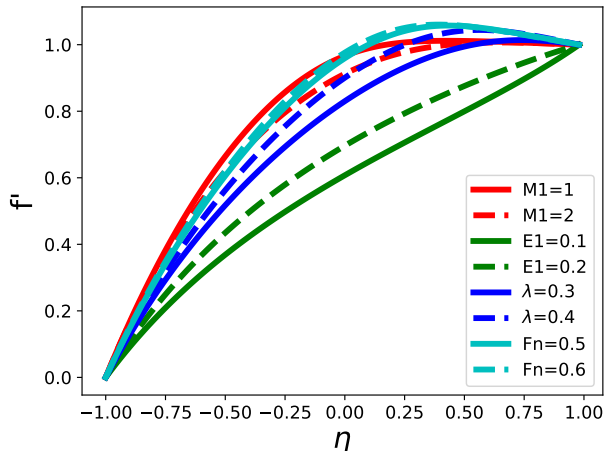
Fig. 2 Influence of M1, E1, λ, and Fn on $f^1(\eta)$.

Fig. 3 Influence of Gr_x, Gc_x on $f^1(\eta)$.

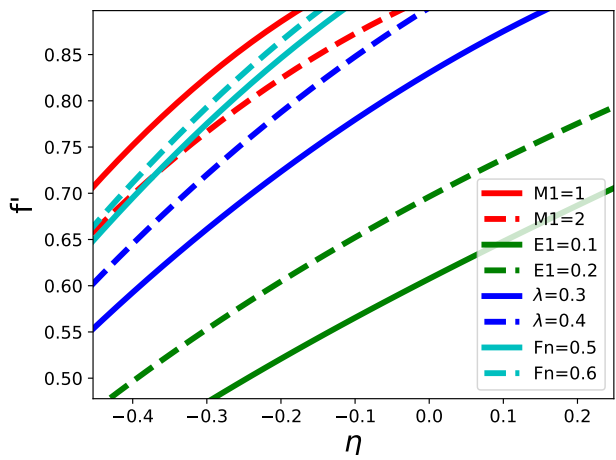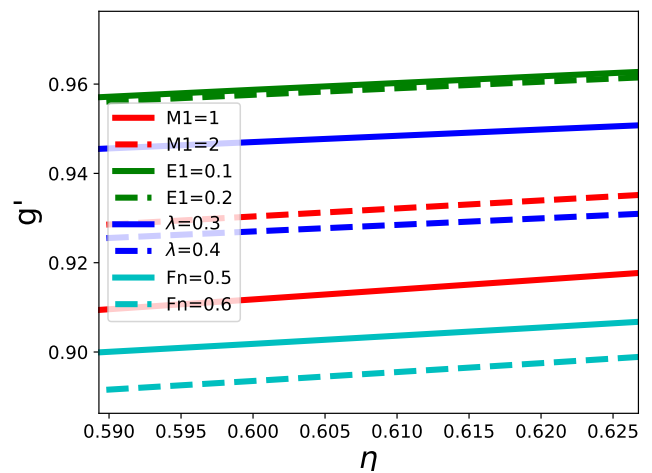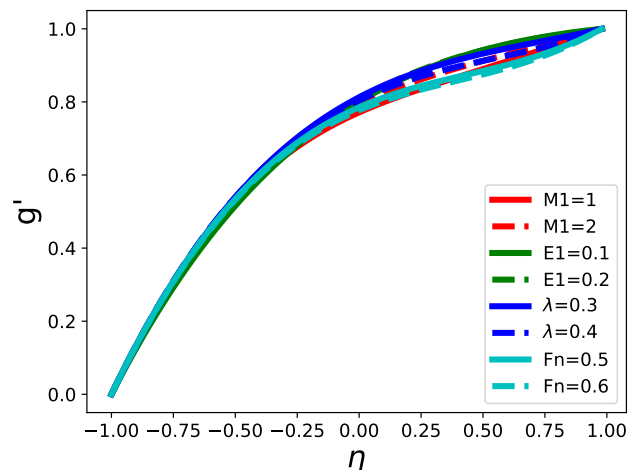**Fig. 4** Influence of M1, E1, λ, and Fn on $g^1(\eta)$.
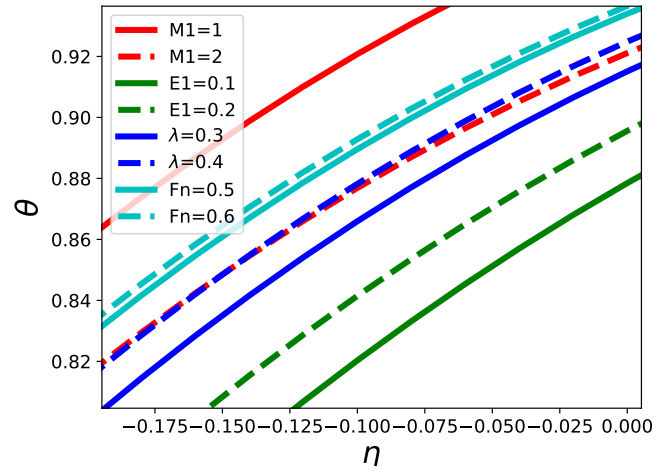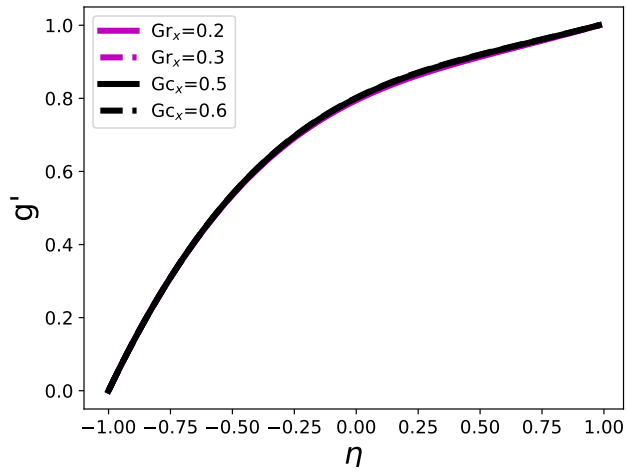
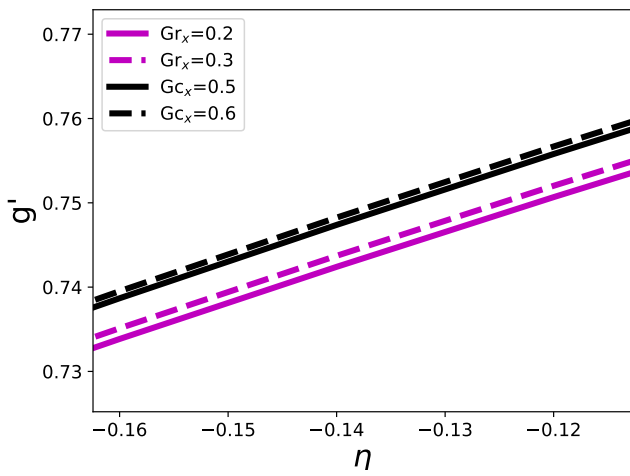**Fig. 6** Influence of M1, E1, λ, and Fn on $\theta(\eta)$.
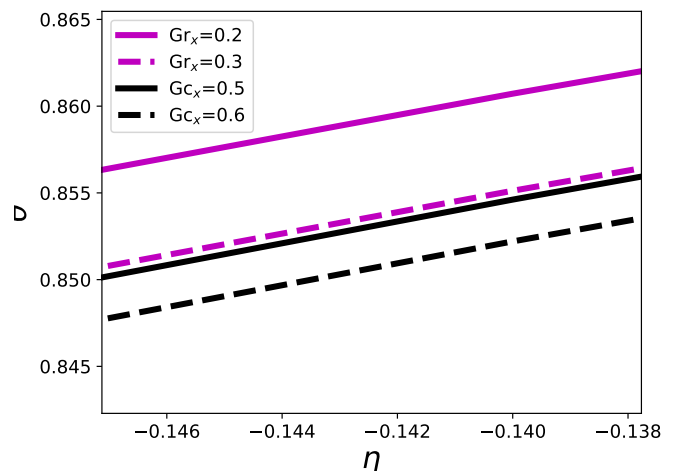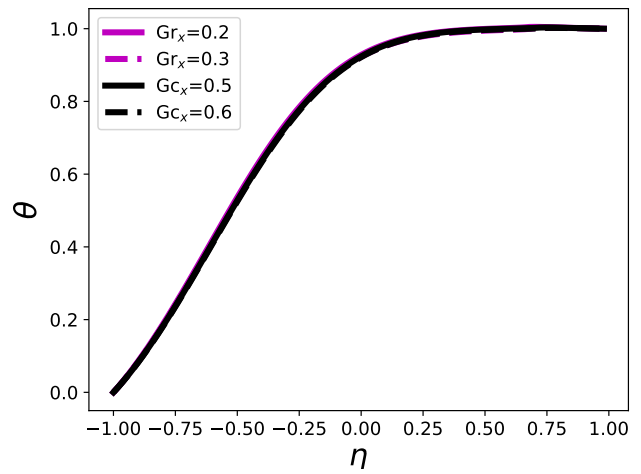

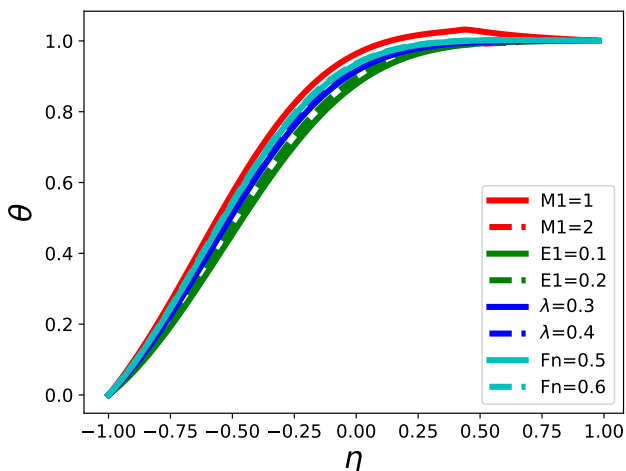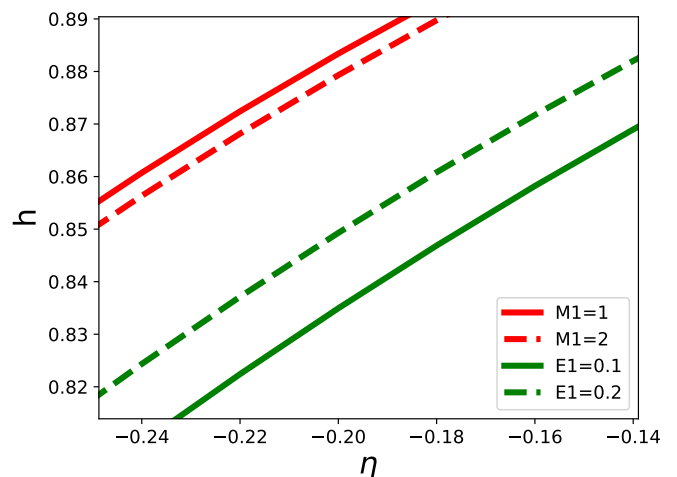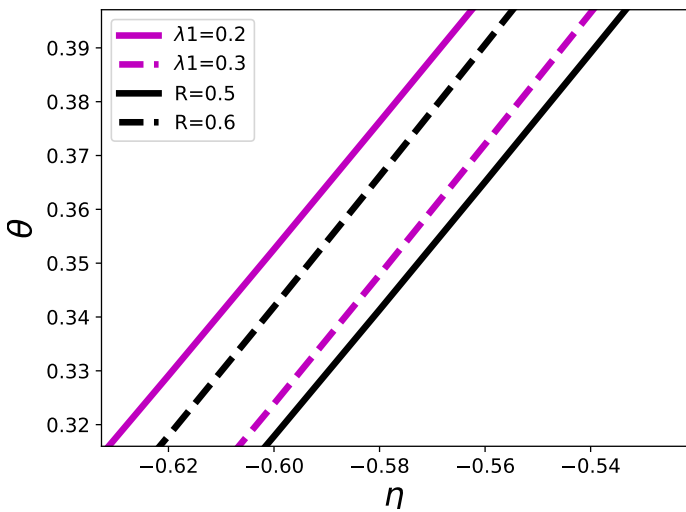**Fig. 5** Influence of Gr$_x$,Gc$_x$ on f$^1(\eta)$.

Fig. 7 Influence of Gr$_x$,Gc$_x$ on $\theta(\eta)$.
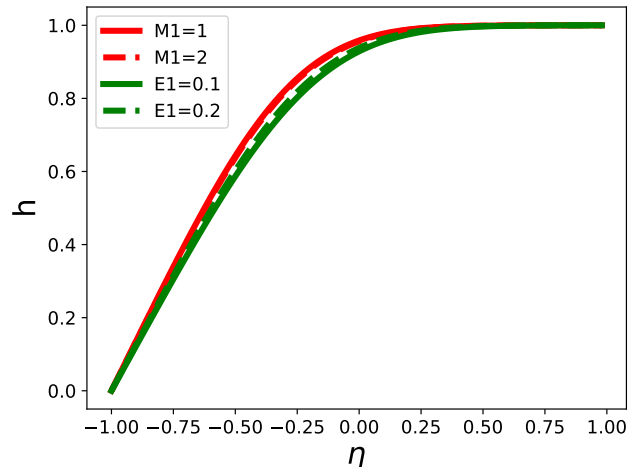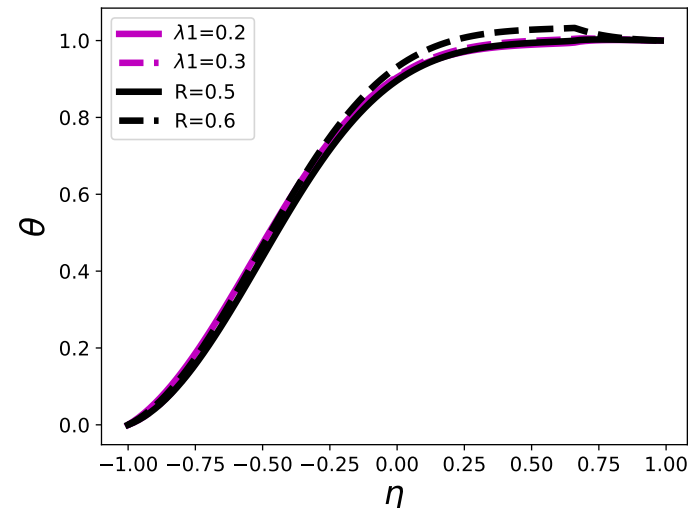
Fig. 9 Influence of M1 and E1 on h(η).
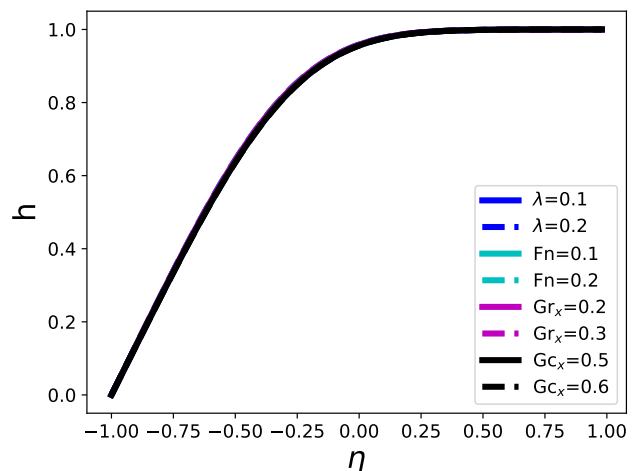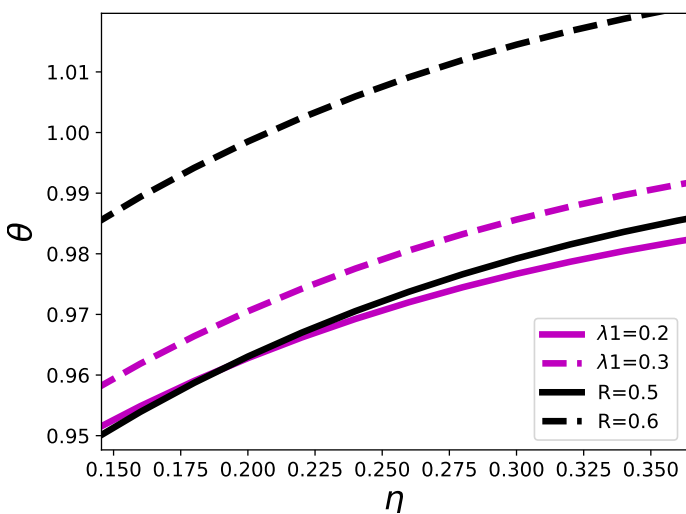
Fig. 8 Influence of R and λ on $\theta(\eta)$.
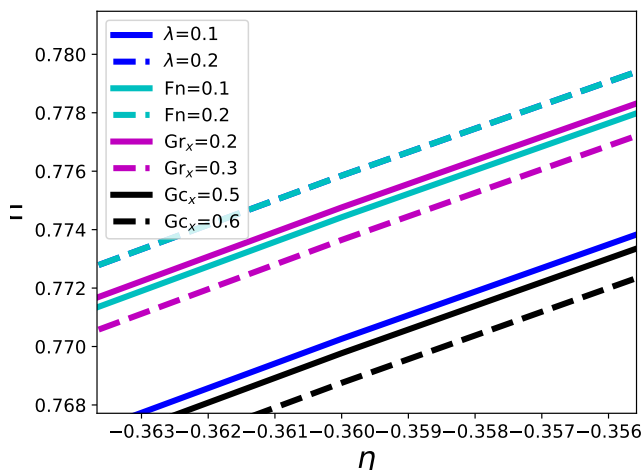
Fig. 10 Influence of λ, Fn, Gr_x, and Gc_x on $h(\eta)$.
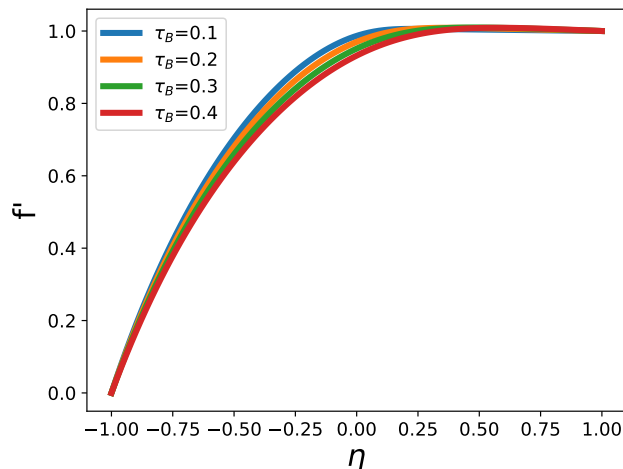
Fig. 12 Influence of Bingham number (τ_B) on Velocity profile.
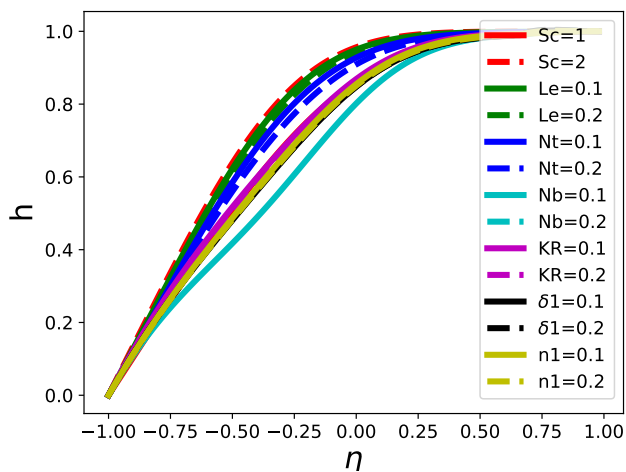
Fig. 11 Influence of Sc, Le, Nt, Nb, KR, $\delta1$, and n1 and E1 on $h(\eta)$.
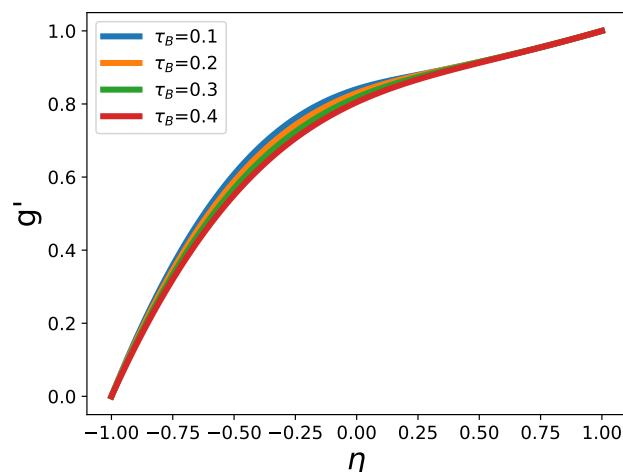
Fig. 13 Influence of Bingham number (τ_B) on Vertical Velocity profile.
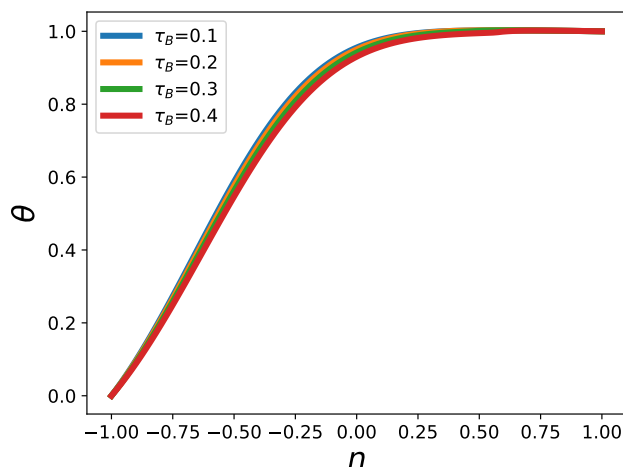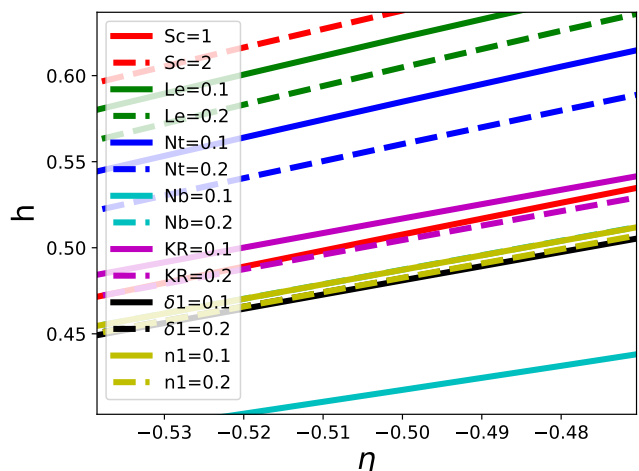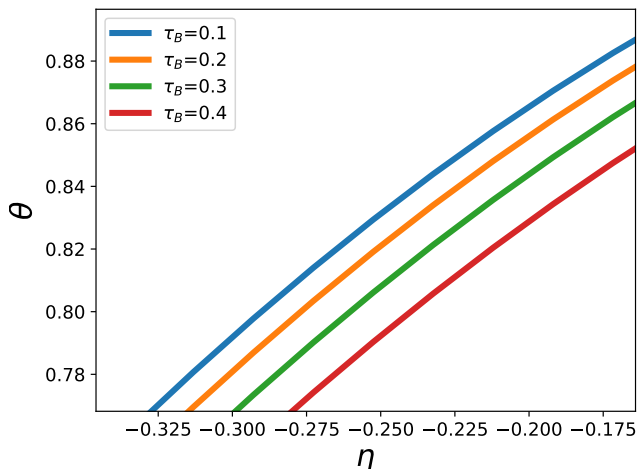
Fig. 14 Influence of Bingham number (τ_B) on Temperature profile.
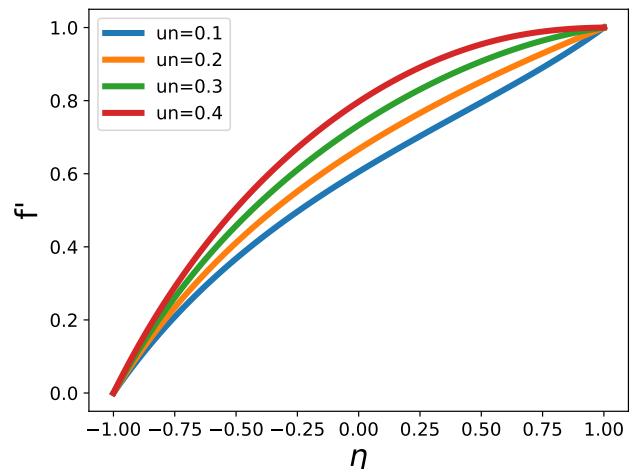
Fig. 16 Influence of unsteady parameter (un) on Velocity profile.
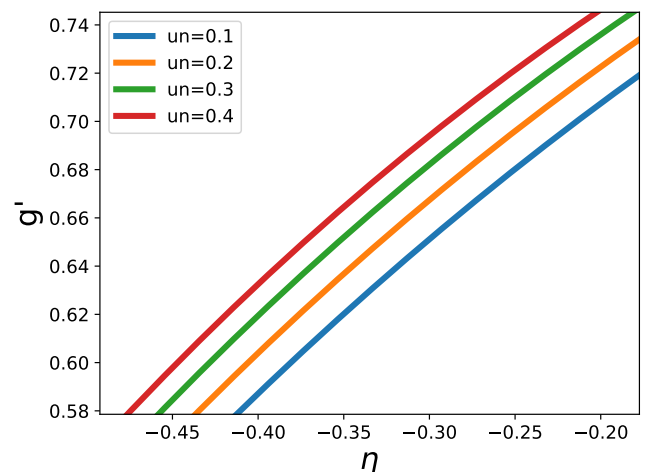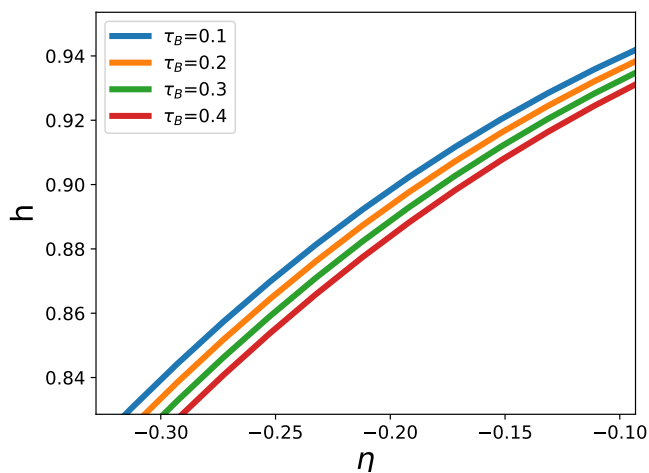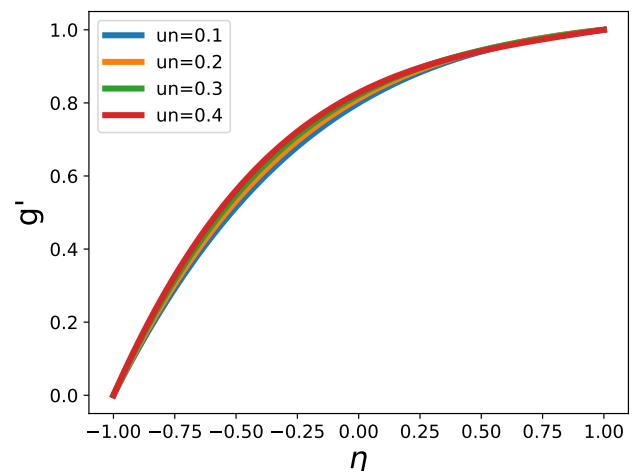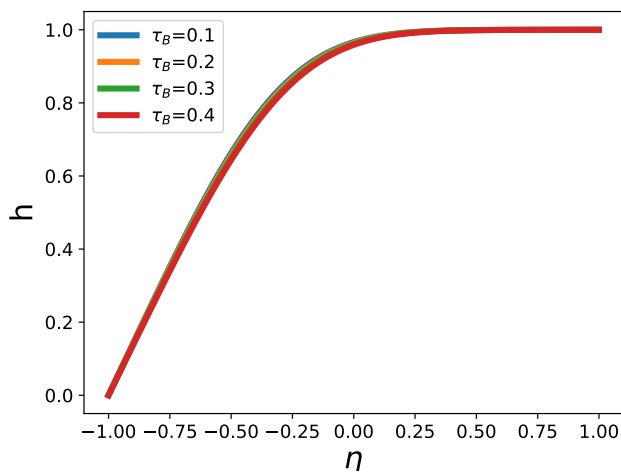
Fig. 15 Influence of Bingham number (τ_B) on Concentration profile.

Fig. 17 Influence of unsteady parameter(un) on Vertical Velocity profile.
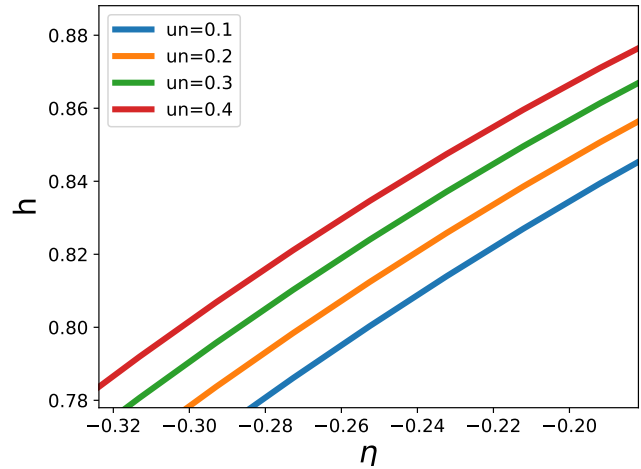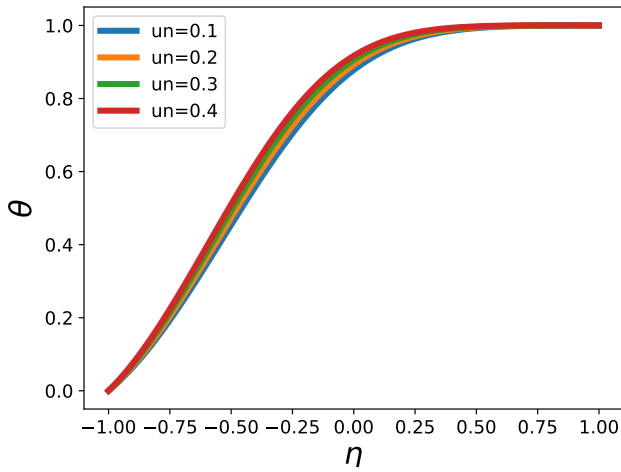
Fig. 19 Influence of unsteady parameter (un) on Concentration profile.
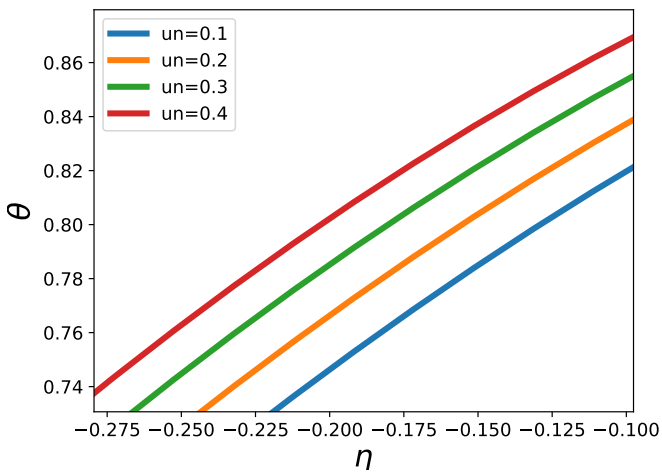
Fig. 18 Influence of unsteady parameter(un) on Temperature profile.
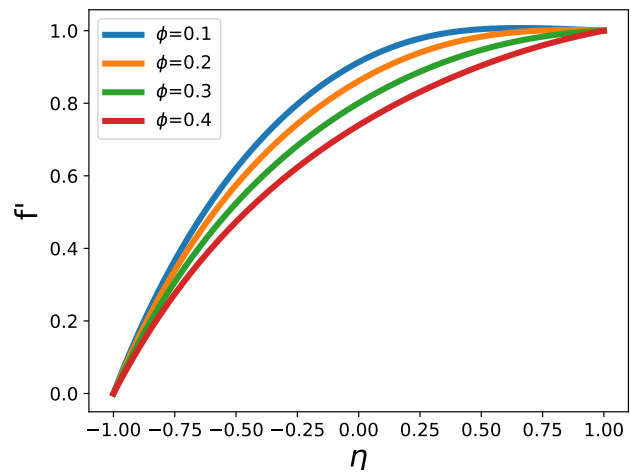
Fig. 20 Influence of volume fraction(ϕ) on Velocity profile.
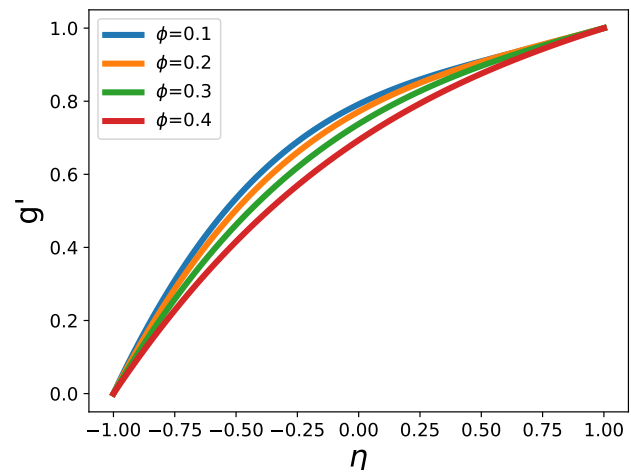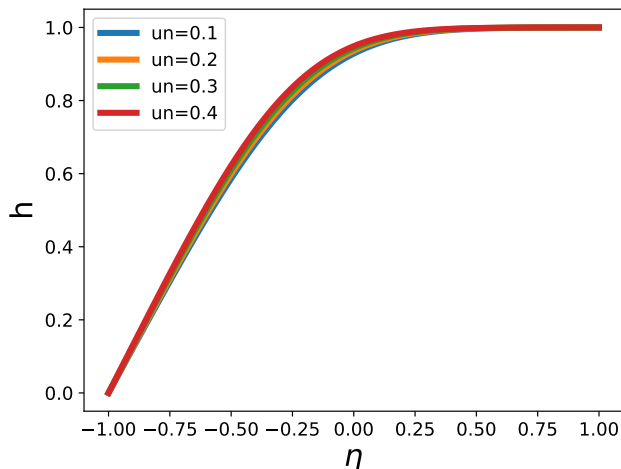
Fig. 21 Influence of volume fraction(ϕ) on Vertical Velocity profile.
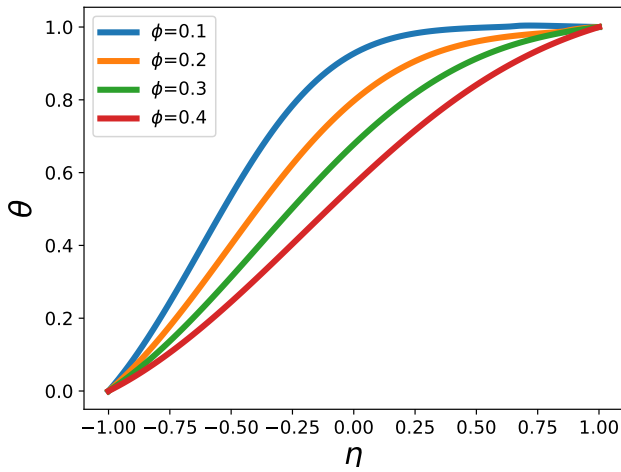
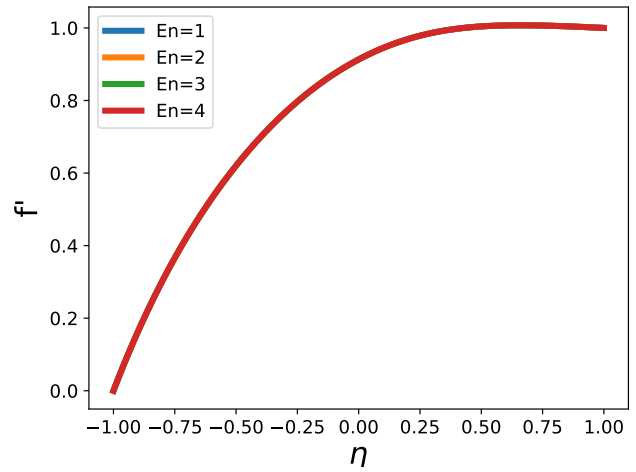**Fig. 22** Influence of volume fraction(ϕ) on Temperature profile.
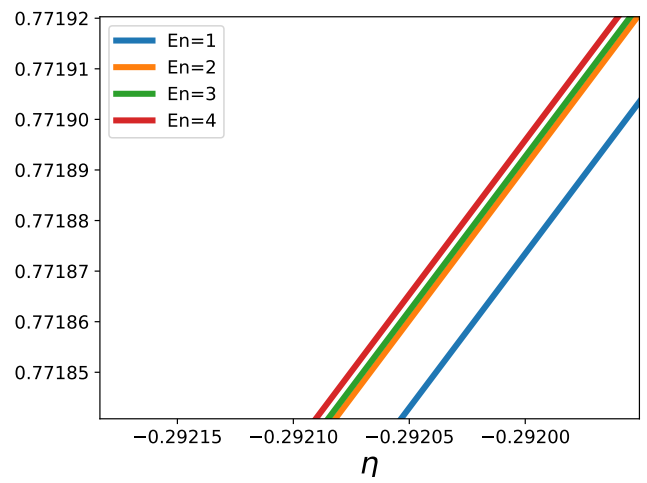
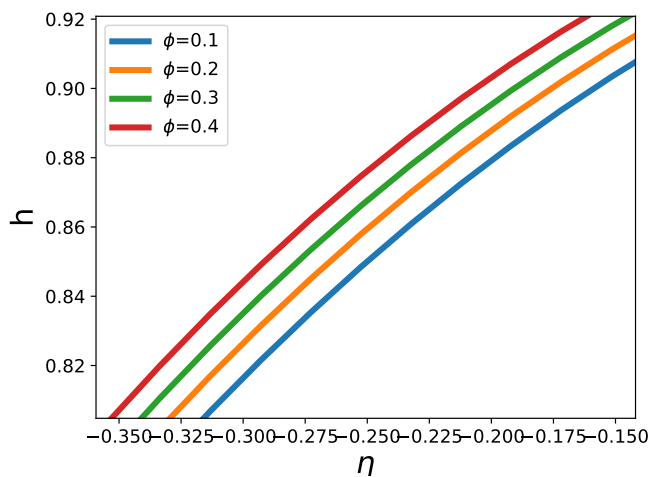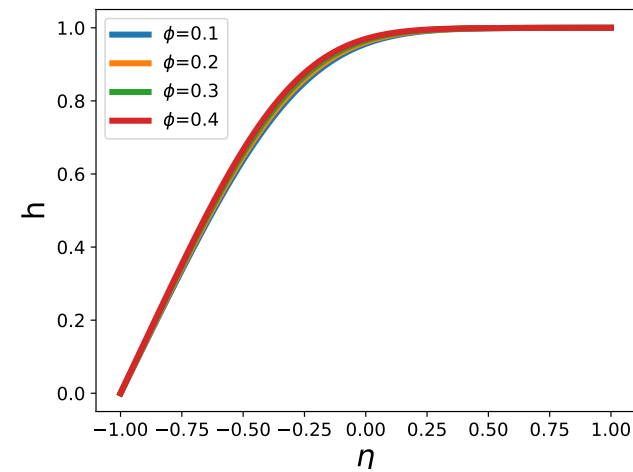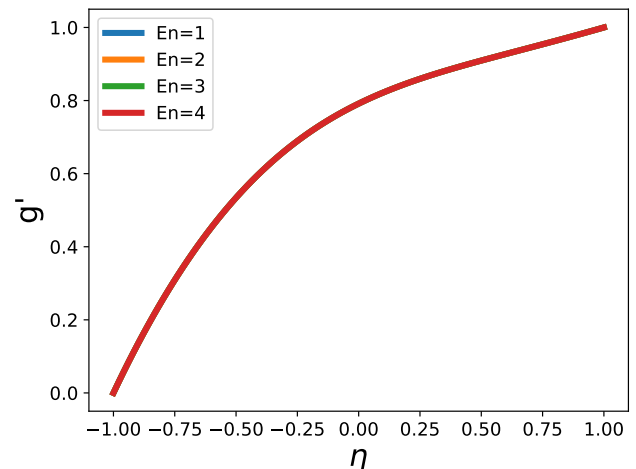**Fig. 24** Influence of activation energy(En) on Velocity profile.

Fig. 23 Influence of volume fraction(ϕ) on Concentration profile.
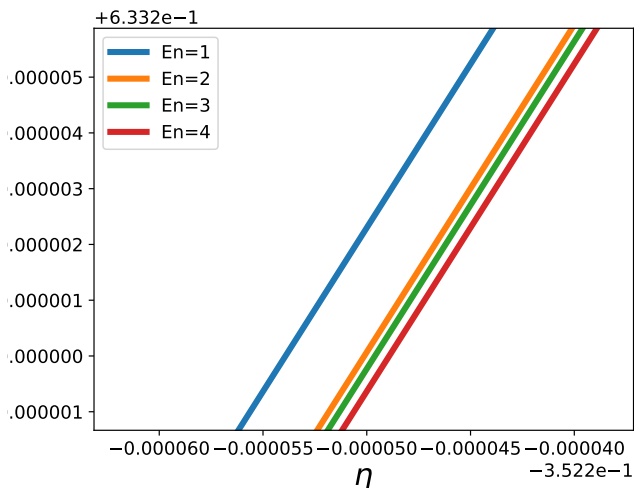
Fig. 25 Influence of activation energy(En) on Vertical Velocity profile.
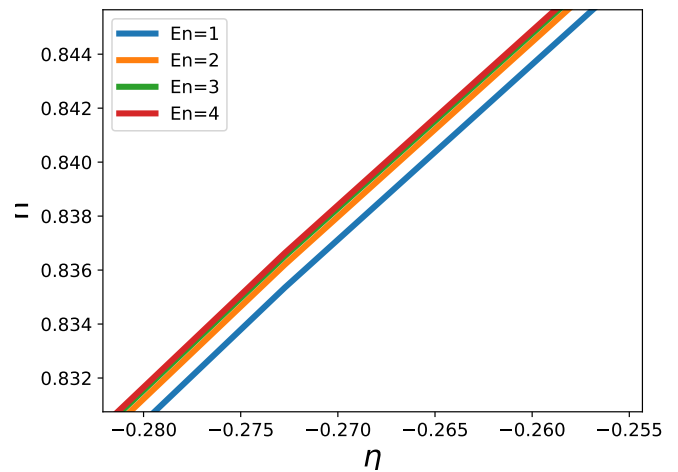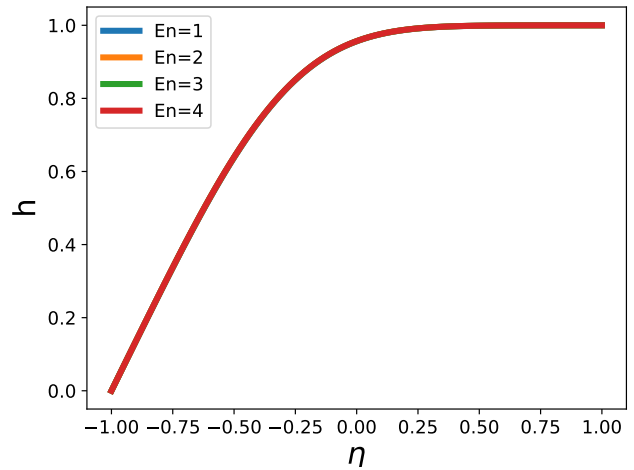

Fig. 27 Influence of activation energy(En) on Concentration profile.
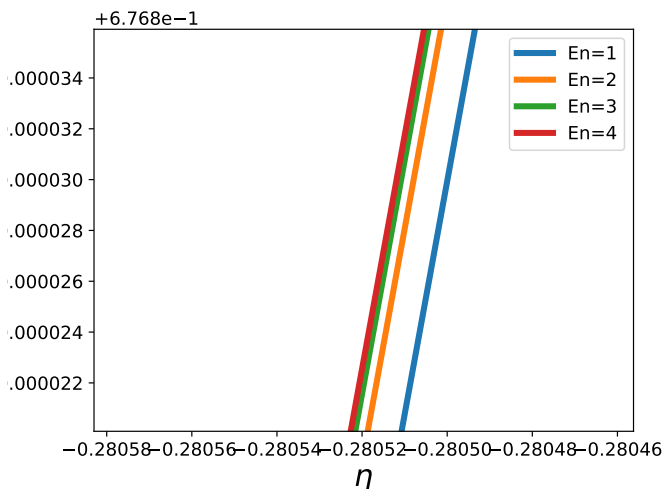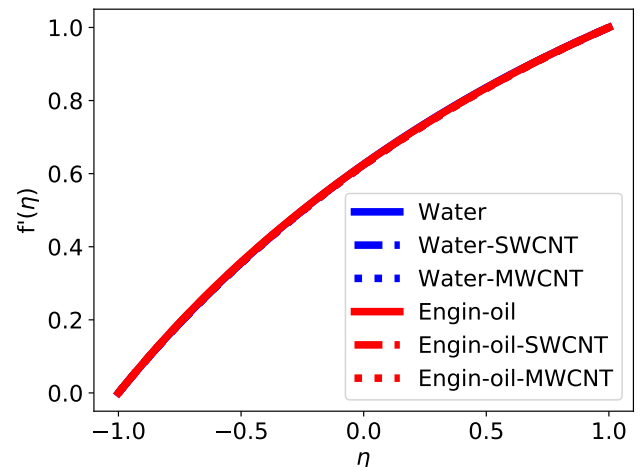

Fig. 26 Influence of activation energy(En) on Temperature profile.

Fig. 28 Velocity profile of water and engin oil explored with SWCNT and MWCNT
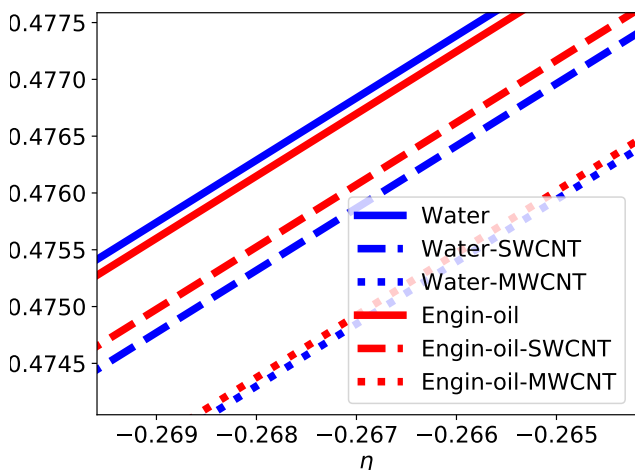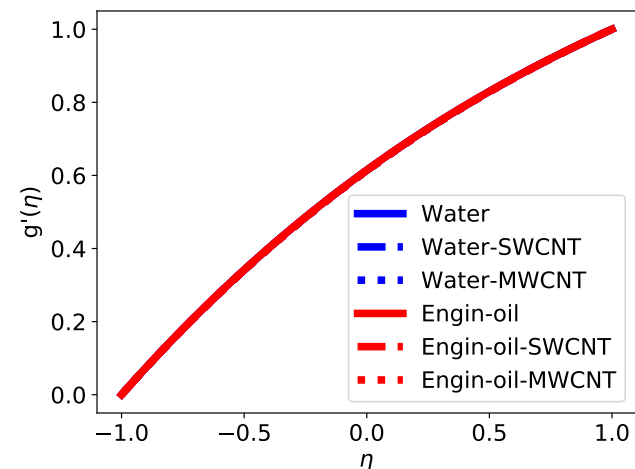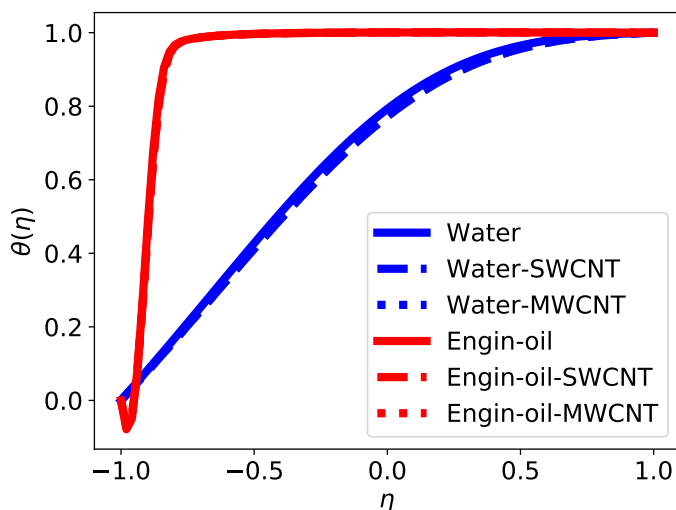
Fig. 29 Vertical Velocity profile of water and engin oil explored with SWCNT and MWCNT

Fig. 30 Temperature profile of water and engin oil explored with SWCNT and MWCNT

Fig. 32 Impact of Bingham number(τ_B)on entropy generation

Fig. 33 Impact of local thermal Peclet number(Pe$_x$)on entropy generation

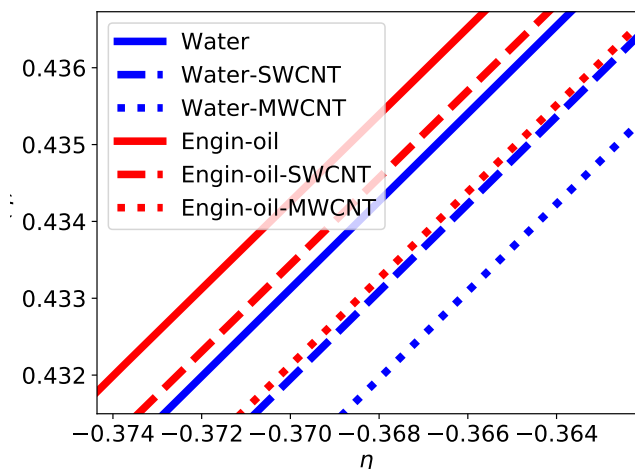**Fig. 31** Concentration profile of water and engin oil explored with SWCNT and MWCNT

Fig. 34 Impact of Fourier number(Fe) on entropy generation

4. CONCLUSIONS

Behavior of Bingham nanofluid with different base fluids of a two-parallel plate system explored with CNTs nearer to the upper and lower plates are studied. The following outcomes are generated as follows.

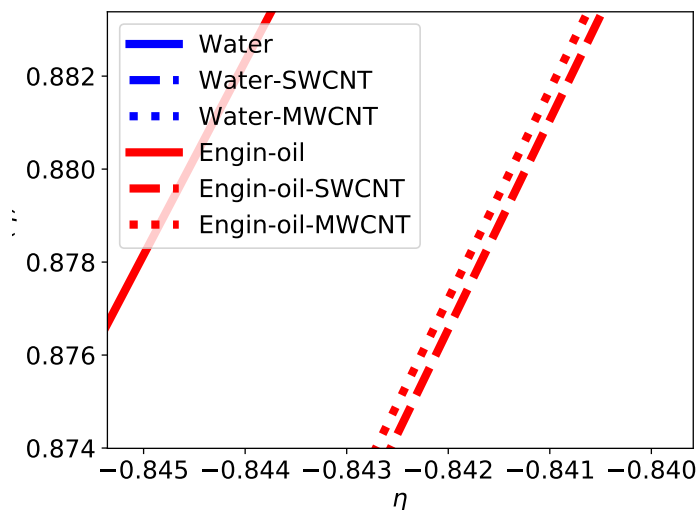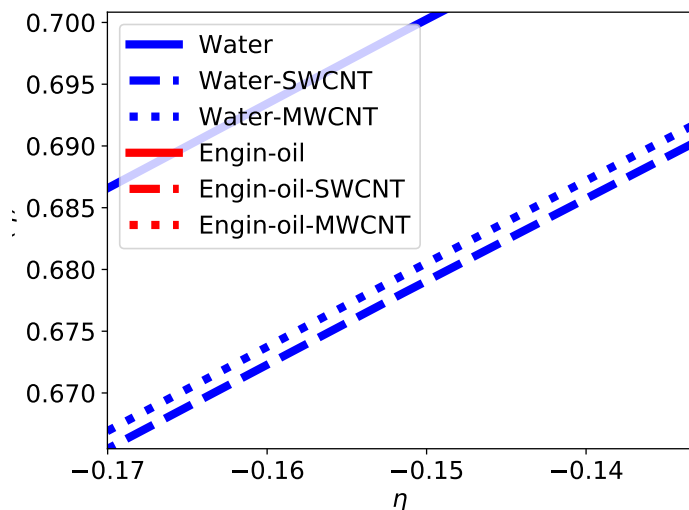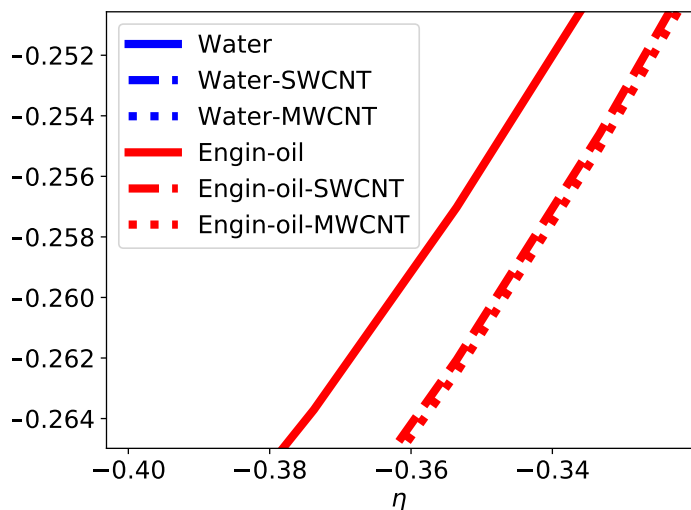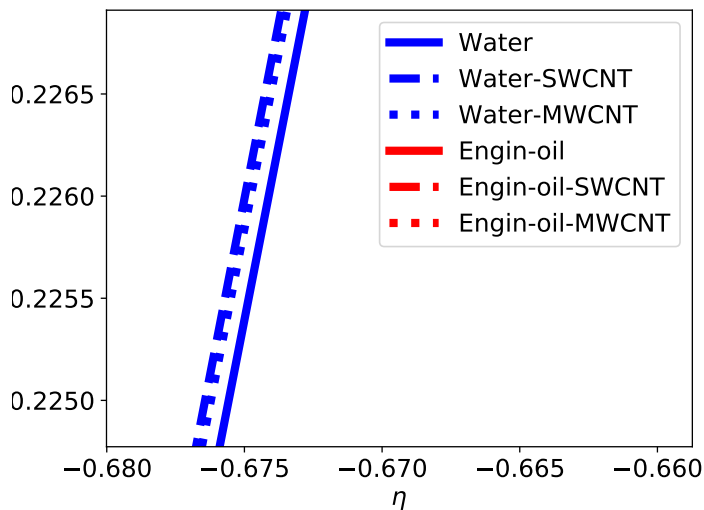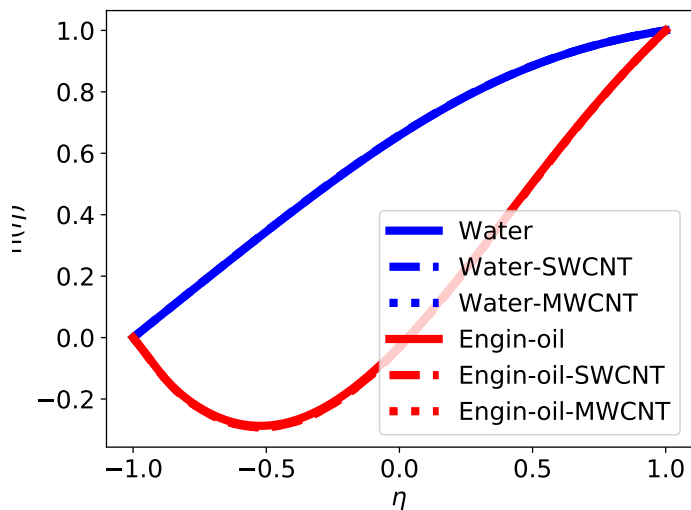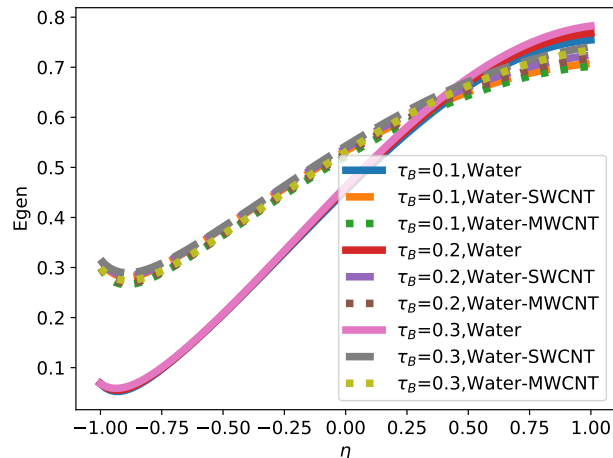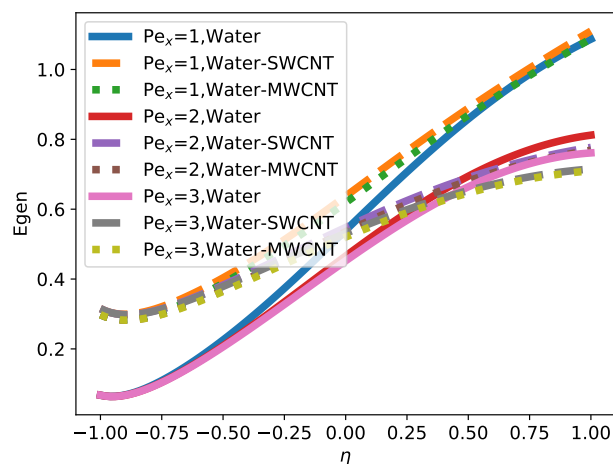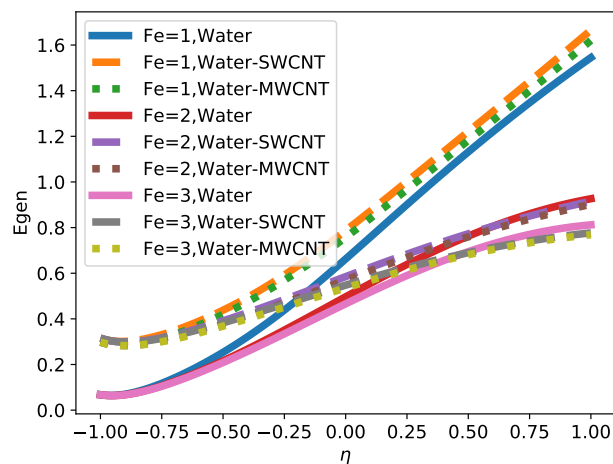- Velocity, temperature and concentration of nanofluid and Bingham number are inversely proportional with each other at the lower plate.

- Velocity, temperature and concentration of nanofluid and unsteady parameter are negatively correlate with each other at the lower plate.

- Velocity, temperature of nanofluid and nanoparticle volume fraction are negatively correlate with each other at the lower plate, but the concentration of nanofluid enhances with the growth tendency of nanoparticle volume fraction.

- Activation energy is directly proportional to horizontal velocity, temperature, and concentration of nanofluid at lower plate.

- Entropy generation of nanofluid with SWCNT dominated as compared to MWCNT under the influence of Bingham number.

- Entropy generation of nanofluid with SWCNT dominated as compared to MWCNT under the influence of diminished value of local thermal Peclet number.

- Entropy generation of nanofluid with SWCNT dominated as compared to MWCNT under the influence of diminished value of Fourier number.

- Rate of heat transfer will increase from fluid to upper plate with increasing local thermal transfer Peclet number and Fourier number once water with CNTs.

- Rate of mass transfer increases from fluid to upper plate with increasing local mass transfer Peclet number and mass transfer Fourier number when engine oil with CNTs.

ACKNOWLEDGEMENTS

NOMENCLATURE

x, y, z	Cartesian Coordinates
p, q, r	Velocity Component in x,y, and z Directions
P, Q	Velocity at the upper plate
$n1$	motile density
ν_{nf}	Kinetic Viscosity of Nanofluid
ν_f	Kinetic Viscosity of Basefluid
ρ_{nf}	Density of Nanofluid
ρ_f	Density of Basefluid
σ_{nf}	Electrical Conductivity of Nanofluid
ρ_f	Electrical Conductivity of Basefluid
B_0	Magnetic Fleld Parameter
E_0	Electric Fleld Parameter
Fn	Inertia-coefficient
$(\beta_T)_{nf}$	Thermal Expansion Coefficient of Nanofluid
$(\beta_T)_f$	Thermal Expansion Coefficient of Basefluid
T_l	Temperature of the fluid at lower plate
T_u	Temperature of the fluid at upper plate
C_u	Concentration of the Fluid at upper plate
C_l	Concentration of the Fluid at lower plate
$(\beta_c)_{nf}$	Concentration Expansion Coefficient of Nanofluid
$(\beta_c)_f$	Concentration Expansion Coefficient of Basefluid
T	Temperature of Fluid
C	Concentration of Fluid
$(C_P)_{nf}$	Specific Heat of Nanofluid
$(C_P)_f$	Specific Heat of Basefluid
D_{nf}	Deficient Coefficient of Nanofluid
D_f	Deficient Coefficient of Basefluid
σ^*	Stephenson Boltzmen Constant
k^*	Rosseland's mean absorption coefficient
K^s	Permeability of Porous Media
η	Similarity Variable
θ	Dimensionless Temperature
h	Dimensionless Concentration
f^1	Velocity (or) Momentum
$(C_P)_{CNT}$	Specific Heat of Carbon Nanotubes
ρ_{CNT}	Density of Carbon Nanotubes
σ_{CNT}	Electrical Conductivity of Carbon Nanotubes
$(\beta_T)_{CNT}$	Thremal Expansion Coefficient of Carbon Nanotubes
$(\beta_C)_{CNT}$	Concentration Expansion Coefficient of Carbon Nanotubes
Gr_x	Local Thermal Grashof Number
GC_x	Local Concentration Grashof Number
$M1$	Magnetic Parameter
$E1$	Electric Parameter
Pr	Preadlt Number
R	Radiation Parameter
λ	Buoyancy
$\lambda1$	Heat Parameter of Source
$\delta1$	Temperature difference parameter
S_c	Smith Number
ϕ	Coefficient of Volume Fraction
α	Source parameter
α_f	Thermal Deficivity Coefficient of Basefluid
a, b	Constant
g	Acceleration due to gravity
Q_0	Coefficient of Heat Source
E	Activation energy
En	Energy activation number
KR	Reaction rate parameter
Nb	Brownian motion parameter
Nt	Thermophoresis parameter
Pe_x	Local thermal Peclet number
Pe_{xm}	Local mass transfer Peclet number
Fe	Heat transfer Fourier number
Fe_m	Mass transfer Fourier number

REFERENCES

Aboud, E., Al-amir, Q., Hamzah, H., Abdulkadhim, A., Gabir, M., Khafaji, S., and Ali, F., 2021, "NATURAL CONVECTON IN SINU-SOIDAL–CORRUGTED ENCLOSURE UTITIING SILVER/WATER NANOLUID WITH DIFFERENT SHAPES OF CONCENTRIC INNER CYLINDERS," *Frontiers in Heat and Mass Transfer*, **17**.
https://doi.org/10.5098/hmt.17.19.

Ahmad, S., Coban, H.H., Khan, M.N., Khan, U., Shi, Q.H., Muhammad, T., Chinram, R., and Kadry, S., 2021, "Computational analysis of the unsteady 3D chemically reacting MHD flow with the properties of temperature dependent transpose suspended Maxwell nanofluid," *Case Studies in Thermal Engineering*, **26**, 101169.
https://doi.org/10.1016/j.csite.2021.101169.

Alexandrou, A.N., Duc, E., and Entov, V., 2001, "Inertial, viscous and yield stress effects in Bingham fluid filling of a 2-D cavity," *Journal of Non-Newtonian Fluid Mechanics*, **96**(3), 383–403.
https://doi.org/10.1016/S0377-0257(00)00199-3.

Ali, R., Shahzad, A., us Saher, K., Elahi, Z., and Abbas, T., 2022, "The thin film flow of Al2O3 nanofluid particle over an unsteady stretching surface," *Case Studies in Thermal Engineering*, **29**, 101695.
https://doi.org/10.1016/j.csite.2021.101695.

Awan, S.E., Khan, Z.A., Awais, M., Rehman, S.U., and Raja, M.A.Z., 2018, "Numerical treatment for hydro-magnetic unsteady channel flow of nanofluid with heat transfer," *Results in Physics*, **9**, 1543–1554.
https://doi.org/10.1016/j.rinp.2018.04.068.

Bayazitoglu, Y., Paslay, P.R., and Cernocky, P., 2007, "Laminar Bingham fluid flow between vertical parallel plates," *International Journal of Thermal Sciences*, **46**(4), 349–357.
https://doi.org/10.1016/j.ijthermalsci.2006.06.008.

Busuioc, V., and Cioranescu, D., 2003, "On the flow of a Bingham fluid passing through an electric field," *International Journal of Non-Linear Mechanics*, **38**(3), 287–304.
https://doi.org/10.1016/S0020-7462(01)00061-0.

Chavez Panduro, E.A., Finotti, F., Largiller, G., and Lervåg, K.Y., 2022, "A review of the use of nanofluids as heat-transfer fluids in parabolic-trough collectors," *Applied Thermal Engineering*, **211**, 118346.
https://doi.org/10.1016/j.applthermaleng.2022.118346.

Chen, C.I., Chen, C.K., and Yang, Y.T., 2004, "Unsteady unidirectional flow of Bingham fluid between parallel plates with different given volume flow rate conditions," *Applied Mathematical Modelling*, **28**(8), 697–709.
https://doi.org/10.1016/j.apm.2003.12.004.

Chen, Y.L., and Zhu, K.Q., 2008, "Couette–Poiseuille flow of Bingham fluids between two porous parallel plates with slip conditions," *Journal of Non-Newtonian Fluid Mechanics*, **153**(1), 1–11.
https://doi.org/10.1016/j.jnnfm.2007.11.004.

Comparini, E., and Mannucci, P., 1998, "Flow of a Bingham Fluid in Contact with a Newtonian Fluid," *Journal of Mathematical Analysis and Applications*, **227**(2), 359–381.
https://doi.org/10.1006/jmaa.1998.6098.

Fusi, L., Farina, A., and Rosso, F., 2012, "Flow of a Bingham-like fluid in a finite channel of varying width: A two-scale approach," *Journal of Non-Newtonian Fluid Mechanics*, **177-178**, 76–88.
https://doi.org/10.1016/j.jnnfm.2012.04.007.

Hasan, H., Sherza, J., Abd, L., Ameena, K., Abed, A., hatem, A., and Sopian, K., 2022, "STUDY THE EFFECT OF FLOW WATER/AL2O3 NANOFLUID INSIDE MINI-CHANNEL FOR COOLING CONCENTRATED MULTI-JUNCTION SOLAR CELL," *Frontiers in Heat and Mass Transfer*, **18**.
https://doi.org/10.5098/hmt.18.45.

Huilgol, R., 2004, "On kinematic conditions affecting the existence and non-existence of a moving yield surface in unsteady unidirectional flows of Bingham fluids," *Journal of Non-Newtonian Fluid Mechanics*, **123**(2), 215–221.
https://doi.org/10.1016/j.jnnfm.2004.08.009.

Huilgol, R., and Mena, B., 2000, "On the time estimate for start-up of pipe flows in a Bingham fluid — a proof of the result due to Glowinski, Lions and Trèmoliéres," *Journal of Non-Newtonian Fluid Mechanics*, **94**(2), 113–118.
https://doi.org/10.1016/S0377-0257(00)00145-2.

Huilgol, R., Mena, B., and Piau, J., 2002, "Finite stopping time problems and rheometry of Bingham fluids," *Journal of Non-Newtonian Fluid Mechanics*, **102**(1), 97–107.
https://doi.org/10.1016/S0377-0257(01)00166-5.

Hussain, M., Mir, F.A., and Ansari, M., 2022, "Nanofluid transformer oil for cooling and insulating applications: A brief review," *Applied Surface Science Advances*, **8**, 100223.
https://doi.org/10.1016/j.apsadv.2022.100223.

Islam, M.M., Mollah, M.T., Khatun, S., Ferdows, M., and Alam, M.M., 2019, "Unsteady Viscous Incompressible Bingham Fluid Flow through a Parallel Plate," *Inventions*, **4**(3).
https://doi.org/10.3390/inventions4030051.

Jiang, W., Song, J., Jia, T., Yang, L., Li, S., Li, Y., and Du, K., 2022, "A comprehensive review on the pre-research of nanofluids in absorption refrigeration systems," *Energy Reports*, **8**, 3437–3464.
https://doi.org/10.1016/j.egyr.2022.02.087.

Kumar, R., Sood, S., Raju, C., and Shehzad, S., 2019, "Hydromagnetic unsteady slip stagnation flow of nanofluid with suspension of mixed bio-convection," *Propulsion and Power Research*, **8**(4), 362–372.
https://doi.org/10.1016/j.jppr.2018.10.001.

Liu, J., Abidi, A., Khan, M.R., Rasheed, S., Allehiany, F., Mahmoud, E.E., and Galal, A.M., 2021, "Thermal analysis of a radiative slip flow of an unsteady casson nanofluid toward a stretching surface subject to the convective condition," *Journal of Materials Research and Technology*, **15**, 468–476.
https://doi.org/10.1016/j.jmrt.2021.08.045.

min WANG, H., ping JIANG, X., min MA, J., and ZHANG, W., 2009, "Vibration of A Single Protein Bubble in Bingham Liquid," *Journal of Hydrodynamics, Ser B*, **21**(5), 658–668.
https://doi.org/10.1016/S1001-6058(08)60197-3.

Oliveira, G.M., Negrão, C.O., and Franco, A.T., 2012, "Pressure transmission in Bingham fluids compressed within a closed pipe," *Journal of Non-Newtonian Fluid Mechanics*, **169-170**, 121–125.
https://doi.org/10.1016/j.jnnfm.2011.11.004.

Osalusi, E., Side, J., Harris, R., and Johnston, B., 2007, "On the effectiveness of viscous dissipation and Joule heating on steady MHD flow and heat transfer of a Bingham fluid over a porous rotating disk in the presence of Hall and ion-slip currents," *International Communications in Heat and Mass Transfer*, **34**(9), 1030–1040.
https://doi.org/10.1016/j.icheatmasstransfer.2007.05.008.

Owayed, J.F., and Tiab, D., 2008, "Transient pressure behavior of Bingham non-Newtonian fluids for horizontal wells," *Journal of Petroleum Science and Engineering*, **61**(1), 21–32.
https://doi.org/10.1016/j.petrol.2007.10.003.

Roussel, N., Lanos, C., and Toutou, Z., 2006, "Identification of Bingham fluid flow parameters using a simple squeeze test," *Journal of Non-Newtonian Fluid Mechanics*, **135**(1), 1–7.
https://doi.org/10.1016/j.jnnfm.2005.12.001.

Sanchez, F., 1998, "Application of a first-order operator splitting method to Bingham fluid flow simulation," *Computers and Mathematics with Applications*, **36**(3), 71–86.
https://doi.org/10.1016/S0898-1221(98)00130-8.

Soleimani, M., and Sadeghy, K., 2011, "Instability of Bingham fluids in Taylor–Dean flow between two concentric cylinders at arbitrary gap spacings," *International Journal of Non-Linear Mechanics*, **46**(7), 931–937.
https://doi.org/10.1016/j.ijnonlinmec.2011.04.003.

Song, Y.Q., Hamid, A., Sun, T.C., Khan, M.I., Qayyum, S., Kumar, R.N., Prasannakumara, B., Khan, S.U., and Chinram, R., 2022, "Unsteady mixed convection flow of magneto-Williamson nanofluid due to stretched cylinder with significant non-uniform heat source/sink features," *Alexandria Engineering Journal*, **61**(1), 195–206. https://doi.org/10.1016/j.aej.2021.04.089.

Spelt, P.M., Yeow, A., Lawrence, C., and Selerland, T., 2005, "Creeping flows of Bingham fluids through arrays of aligned cylinders," *Journal of Non-Newtonian Fluid Mechanics*, **129**(2), 66–74. https://doi.org/10.1016/j.jnnfm.2005.05.007.

Tang, G., Wang, S., Ye, P., and Tao, W., 2011, "Bingham fluid simulation with the incompressible lattice Boltzmann model," *Journal of Non-Newtonian Fluid Mechanics*, **166**(1), 145–151. https://doi.org/10.1016/j.jnnfm.2010.11.005.

Tokpavi, D.L., Jay, P., and Magnin, A., 2009, "Interaction between two circular cylinders in slow flow of Bingham viscoplastic fluid," *Journal of Non-Newtonian Fluid Mechanics*, **157**(3), 175–187. https://doi.org/10.1016/j.jnnfm.2008.11.001.

Vola, D., Boscardin, L., and Latché, J., 2003, "Laminar unsteady flows of Bingham fluids: a numerical strategy and some benchmark results," *Journal of Computational Physics*, **187**(2), 441–456. https://doi.org/10.1016/S0021-9991(03)00118-9.

Wilkens, R., Miller, J., Plummer, J., Dietz, D., and Myers, K., 2005, "New techniques for measuring and modeling cavern dimensions in a Bingham plastic fluid," *Chemical Engineering Science*, **60**(19), 5269–5275. https://doi.org/10.1016/j.ces.2005.04.058.

Yang, S.P., and Zhu, K.Q., 2006, "Analytical solutions for squeeze flow of Bingham fluid with Navier slip condition," *Journal of Non-Newtonian Fluid Mechanics*, **138**(2), 173–180. https://doi.org/10.1016/j.jnnfm.2006.05.007.

Yun, H., Lv, S., and Wu, S., 2022, "EXPERIMENTAL RESEARCH ON THE HEAT TRANSFER CHARACTERISTICS OF NANOFLUIDS IN CRUDE OIL HEATING FURNACE," *Frontiers in Heat and Mass Transfer*, **18**. https://doi.org/10.5098/hmt.18.3.

Zhang, G., Wang, Y., and Ma, J., 2002, "Bingham plastic fluid flow model for ceramic tape casting," *Materials Science and Engineering: A*, **337**(1), 274–280. https://doi.org/10.1016/S0921-5093(02)00043-6.

Zhang, J., 2010, "An augmented Lagrangian approach to Bingham fluid flows in a lid-driven square cavity with piecewise linear equal-order finite elements," *Computer Methods in Applied Mechanics and Engineering*, **199**(45), 3051–3057. https://doi.org/10.1016/j.cma.2010.06.020.

Zhu, H., Martys, N.S., Ferraris, C., and Kee, D.D., 2010, "A numerical study of the flow of Bingham-like fluids in two-dimensional vane and cylinder rheometers using a smoothed particle hydrodynamics (SPH) based method," *Journal of Non-Newtonian Fluid Mechanics*, **165**(7), 362–375. https://doi.org/10.1016/j.jnnfm.2010.01.012.